Article

### Ferrocene-Containing Desmuramylpeptides Adopt A Flexible Conformation and Exhibit NOD2 Agonistic Activity

Željka Car, Monika Kovačević, Vesna Petrović Peroković, Karla Čižmešija, Rosana Ribić, Špela Janež, Ziga Jakopin,\* and Lidija Barišić\*



Cite This: Organometallics 2025, 44, 2440-2456



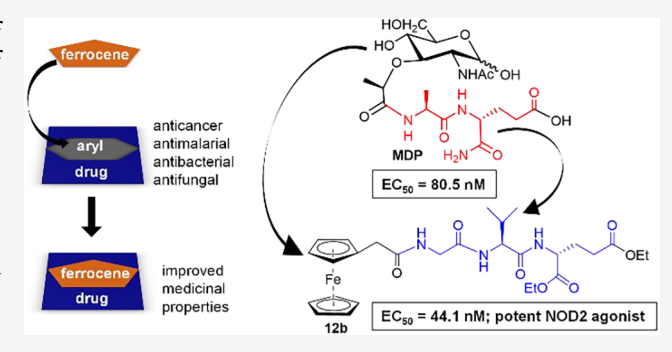
**ACCESS** I

III Metrics & More

Article Recommendations

Supporting Information

ABSTRACT: This study extends our preliminary investigation of ferrocene-containing desmuramylpeptides as potential agonists of nucleotide binding oligomerization domain containing protein 2 (NOD2). We report the rational design, chemical synthesis, conformational characterization and biological evaluation of 13 novel ferrocene conjugates with the desmuramyldipeptide L-Ala-D-isoGln (10c/g, 11a-c, 13d/f) and tripeptide Gly-L-Val-D-Glu-(OEt)<sub>2</sub> (12a-f). Detailed spectroscopic analysis revealed the presence of conformationally flexible structures driven by weak intramolecular hydrogen bonds. The ferrocene-carrying desmuramylpeptides were evaluated for their in vitro NOD2 agonist activity on the HEK-Blue NOD2 reporter cell. Of the ferrocene



derivatives tested, conjugates 12b and 12c exhibited the strongest NOD2 agonist activity of the series, with the lowest EC50 values of 44.1 and 252.6 nM, respectively. The best performing compound 12b also induced cytokine production in peripheral blood mononuclear cells (PBMCs), both alone and in combination with lipopolysaccharide (LPS). This work thus presents the first potent ferrocene-modified NOD2 agonists and provides a framework for the rational design and further optimization of ferrocene-based NOD2 immunomodulators.

#### 1. INTRODUCTION

Ferrocene has been extensively studied in the field of molecular chemistry and material science due to its remarkable stability and aromatic electrophilicity, reversible and mild redox behavior, solubility in organic solvents, air stability and lipophilic nature.<sup>1,2</sup> Although the idea of substituting aryl moieties in pharmaceutical compounds with ferrocene as bioisosteric analogues was introduced in the 1970s,3 the significant advances in ferrocene-based medicinal chemistry were not achieved until two decades later. In 1997, Jaouen et al.5 reported the synthesis of a ferrocene analogue of hydroxytamoxifen, which showed pronounced antitumor activity in both hormone-dependent and hormone-independent breast cancer cell lines. At the same time Biot et al.6 published the synthesis of a ferrocene analogue of chloroquine, which showed superior efficacy against malaria compared to its parent compound. In addition to tamoxifen, the incorporation of ferrocene as a bioisosteric motif has been shown to enhance the anticancer properties of a wide range of pharmacologically active compounds.7 This strategy has also been used in the development of potent antimicrobial and antioxidant agents.<sup>7,8</sup> Considering the broad spectrum of biological activities conferred by ferrocene as a bioisosteric motif, its incorporation into drug molecules and bioactive scaffolds represents a promising approach for the development of novel and

efficacious therapeutic agents.<sup>7,9,10</sup> Recently, ferrocene was proposed to constitute a "privileged" scaffold for the design of ligands and catalysts in asymmetric synthesis.<sup>11</sup>

We have shown that mono- and 1,1'-disubstituted ferrocene scaffolds induce stable turn- and  $\beta$ -sheet-like structures upon conjugation with amino acids and small peptides. In addition to the effects of ferrocene scaffold, the steric hindrances of the amino acid side chains and the bulkiness and basicity of the Nprotecting groups also have a strong influence on the conformational properties of ferrocene peptides. 12,13 The cytotoxic activity of the previously described ferrocenecontaining peptides increased mainly with lipophilicity, but also depended on the treated cell line. There was also no clear relationship between the assumed conformational motif and the cytotoxic activity. 14-19

In addition to the aforementioned antitumor, antimicrobial, and antioxidant properties of ferrocene derivatives, it has been shown that conjugating ferrocene units with steroids,  $\beta$ -

Received: August 19, 2025 Revised: October 8, 2025 Accepted: October 9, 2025 Published: October 14, 2025





Figure 1. Structures of (a) MDP, (b) ferrocene-containing desmuramyldipeptides (X = O, NH; n = 2, 4)<sup>36</sup> (c) trans-ferulic acid based desmuramyltripeptide SG8<sup>34</sup> and (d) novel ferrocene-carrying desmuramyldi- (10c/g, 11a-c, 13d/f) and tripeptides 12a-f.

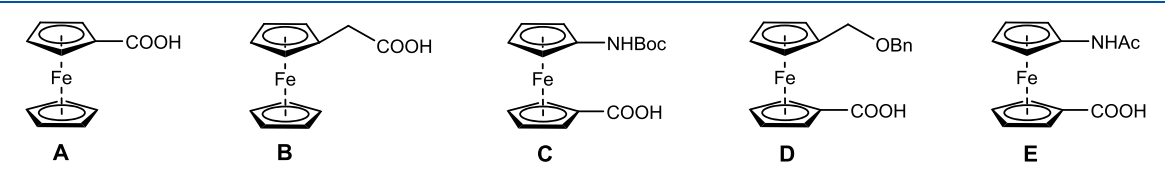


Figure 2. Ferrocene scaffolds A-E as precursors of goal compounds 10c/g, 11a-c, 13d/f and 12a-f.

cyclodextrin, and hydrazones can induce immunomodulatory effects.  $^{20-22}$  In this study, we present our contribution to the development of ferrocene-based immunomodulatory agents, specifically those acting as NOD2 agonists.

NOD2 belongs to the family of NOD-like receptors for pathogen recognition and its activation triggers the immune signaling, which is responsible for the activation of NF- $\kappa$ B and MAPK pathways and the production of various immune effectors such as cytokines. <sup>23–26</sup> MDP (*N*-acetylmuramyl–L-Ala-D-isoGln) (Figure 1a) is the minimal peptidoglycan fragment found in almost all bacteria that acts as a key ligand for NOD2. The direct binding of MDP to NOD2 via its LRR domain was first demonstrated biochemically by Lauro et al.<sup>2</sup> Structure-activity relationship (SAR) studies have confirmed that the chemical modification of MDP can improve its pharmacological properties, 28 and the promising strategy involves substitution of the N-acetylmuramyl moiety (Mur-NAc) with appropriate bioisosteres to increase lipophilicity, which plays a crucial role in modulating biological activity in vivo. The resulting desmuramylpeptides generally retain the conserved or slightly modified MDP peptide motif (such as L-Ala-D-isoGln, L-Ala-D-Glu, or Gly-L-Val-D-Glu) decorated with various lipophilic substituents. Recently, we successfully prepared the first ferrocene-containing desmuramylpeptides (Figure 1b). The molecular docking study, modeling their interactions with the NOD2 receptor, revealed that the most promising candidate contains the ferrocene moiety conjugated to the γ-carboxyl group of the L-Ala-DisoGln dipeptide via an amide bond through a butyl linker (X = NH, n = 4) (Figure 1b).<sup>35</sup> Notably, the most potent desmuramylpeptide analogue reported to date incorporate an aromatic *trans*-ferruloyl moiety attached to the tripeptide Gly–L-Val–D-Glu (compound **SG8**; Figure 1c), exhibiting NOD2 agonist activity at low nanomolar concentrations.<sup>32,34</sup>

Inspired by the notable agonist activity of aromatic desmuramylpeptides and acknowledging the considerable therapeutic potential of ferrocene-conjugated pharmacophores, 5-10,36 we aimed to investigate whether replacing the MurNAc moiety in MDP and the *trans*-ferruloyl moiety in SG8 with a ferrocene unit could enhance the activity of the resulting analogues. Accordingly, we designed and synthesized ferrocene-based conjugates with L-Ala-D-isoGln (10c/g, 11a-c, 13d/f) and Gly-L-Val-D-Glu (12a-f), and evaluated their immunomodulatory activity (Figure 1d, Scheme 2).

The key aspects addressed in this study include: (i) the ability of the ferrocene-containing desmuramylpeptides to establish strong intramolecular hydrogen bonds and adopt a stable folded conformation, (ii) the capacity of ferrocene to act as an aromatic surrogate of the MurNAc moiety in the development of novel NOD2 agonists, (iii) the structure—activity relationship of ferrocene-carrying desmuramylpeptides as NOD2 agonists.

#### 2. RESULTS AND DISCUSSION

2.1. Synthesis of Ferrocene-Conjugated Desmuramylpeptides. The ferrocene carboxylic acids A-E, which are required for the preparation of the goal dipeptides 10c/g, 11a-c, and 13d/f as well as tripeptides 12a-f, are shown in Figure 2.

#### Scheme 1. Preparation of Ferrocene Precursors D and E<sup>a</sup>

<sup>a</sup>(a) 1. SOCl<sub>2</sub>, dry DCM; 2. pyridine, reflux, 2 h; (b) NaBH4, dry THF, MeOH dropwise, 1.5 h, 80%; (c) BnBr, Ag<sub>2</sub>O, 6 days, 76%; (d) 1. NaOH 1M, 1,4-dioxane, 24 h; 2. HCl<sub>aq</sub>, 91% for D, 82% for E, 67% for C; (e) TFA, dry DCM, 1.5 h; 68%; (f) AcCl, pyridine, dry DCM, 1 h, 75%

The synthesis of the novel substituted ferrocene scaffolds D and E is shown in Scheme 1. The alcohol 2 was prepared by treating the carboxylic group of 1 with SOCl<sub>2</sub> in pyridine via an unstable ferrocenyl chloride, which was used as crude material in the next step. It was treated with NaBH4 with gradual addition of MeOH to give the desired alcohol 2 in good yield (80%, calculated from 1). The lipophilic benzyl protecting group was incorporated into 2 using benzyl bromide and Ag<sub>2</sub>O as base. The reaction proceeded slowly (6 days) but resulted in a satisfactory yield of the benzyl ether 3 (76%). We also investigated other conditions as a faster alternative for this step by using NaH in dry DMF as solvent, which resulted in a shorter reaction time (48 h) and a slightly lower yield of 3 (55%). Carboxylic acid D was obtained by saponification with an aqueous solution of NaOH in 1,4-dioxane and subsequent acidification in 91% yield. The same procedure was used for the conversion of the Boc-protected 4 to precursor C and the amide derivative 6 to acid E, which were obtained in good yields of 67 and 82%, respectively. Compound 4 was subjected to standard trifluoroacetic acid-mediated acidolysis to remove the Boc protecting group, yielding 5 (68%). Finally, the amide derivative 6 was obtained by acetyl chloride in pyridine, a short reaction that gave 6 in very good yield (75%) (Scheme 1).

The desmuramylpeptide building blocks L-Ala-D-isoGln-(OBn) 7, L-Ala-D-isoGln(OtBu) 8 and Gly-L-Val-D-Glu-(OEt)<sub>2</sub> 9 which are required for the conjugation with ferrocene acids A - E were prepared according to previously published procedures. 29,37,38 The goal ferrocene dipeptides 10c/g, 11ac, 13d/f and the tripeptides 12a-f were synthesized as shown in Scheme 2. The coupling step was performed using the standard EDC/HOBt methodology and resulted in moderate to good overall yields (45-77%). Compounds 11a-c with the debenzylated  $\gamma$ -carboxylic group of isoGln as well as 12f and 13f with a deprotected hydroxyl group of the ferrocene moiety were obtained from their benzyl-protected counterparts (10ac and 12d/13d) by hydrogenolysis in very good to high yields (50-92%). The conjugate 10g was prepared from 10c by TFA-mediated acidolysis and subsequent removal of the trifluoroacetic counterion.

**2.2.** Conformational Analysis of Ferrocene-Conjugated Desmuramylpeptides. To prevent the solvent from interfering with the hydrogen bonding arrangement in the peptides analyzed, the conformational analysis is performed in a nonpolar CDCl<sub>3</sub>. Therefore, peptides **12a**–**f**, which are readily soluble in CDCl<sub>3</sub>, were selected for detailed conforma-

tional characterization. Conversely, the peptides that were only soluble in hydrogen bond competing solvents such as MeOH and DMSO (10g, 11a-c and 13f) or had limited solubility in CDCl<sub>3</sub> at room temperature (10c and 13d) were excluded from the conformational analysis.

IR spectroscopy is widely utilized to examine the role of hydrogen bonding in modulating the conformational behavior of peptides and proteins.<sup>39-41</sup> When N-H and C=O groups are involved in hydrogen bonding, their IR vibrational modes generally exhibit increased intensity and are red-shifted. 42-45 Consequently, the appearance of red-shifted N-H (~3300-3330 cm<sup>-1</sup>) and C=O (~1660 cm<sup>-1</sup>) bands in IR spectra of 12a-f serves as a spectroscopic signature of N-H···O=C hydrogen bonding within peptides (Figure 3). When analyzing the ratio of free (~3413-3437 cm<sup>-1</sup>) and associated NH groups (~3300-3330 cm<sup>-1</sup>), a predominance of nonbonded states is observed in the monosubstituted conjugate 12a, while the prevalence of hydrogen-bonded states is evident only in the disubstituted conjugates 12c and 12e. Conversely, an approximately equal distribution of free and bonded states is observed in the remaining three conjugates analyzed (12b, 12d and 12f).

In addition to the band position and the band intensity, the bandwidth also provides valuable information. Given the short characteristic time scale, IR spectroscopy captures a snapshot of the conformations present in the sample. As the vibrational frequency and thus the band position varies slightly between different conformers, this leads to a broadening of the band. Therefore, more flexible structures have broader bands than more rigid ones, so that the bandwidth is an indicator of the conformational flexibility. The broadening of the NH region of peptides 12a-f (especially the NH region of 12c with an additional blue-shifted shoulder at 3437 cm<sup>-1</sup>) thus indicates a conformational flexibility resulting from their involvement in weaker hydrogen bonds (Figure 3).

To clarify the nature of hydrogen bonding - whether intraor intermolecular - we obtained the IR spectra of peptides 12a-f over a range of concentrations ( $5 \times 10^{-2}$  M,  $2.5 \times 10^{-2}$  M,  $1.25 \times 10^{-2}$  M,  $6.13 \times 10^{-3}$  M,  $3 \times 10^{-3}$  M) (Figure 3). If the hydrogen bonds are intramolecular, dilution should not alter the ratio of bonded to nonbonded NH bands. In contrast, a decrease in the intensity of associated NH bands relative to free NH bands upon dilution indicates the presence of intermolecular aggregates. A  $\sim$ 30% increase in the free-toassociated NH band ratio observed for peptides 12a, 12c and

## Scheme 2. Preparation of the Goal Ferrocene Conjugates with (a) Desmuramyldipeptides 7 and 8 and (b) Desmuramyltripeptide $9^a$

(a)

(b)

#### Scheme 2. continued

<sup>a</sup>Either of carboxylic acids **A**–**E**, EDC × HCl, HOBt, TEA, dry DCM, 0 °C, 1h; 2. rt, 48h, 77% for **10a**, 45% for **10b**, 60% for **10c** and **12a**, 52% for **12b**, 62% for **12c**, 70% for **12d**, 77% for **12e**, 71% for **13d**; (b) H<sub>2</sub>, 10% Pd/C, MeOH, 3 bar, 2h, 90% for **11a** and **13f**, 50% for **11b**, 92% for **11c**, 75% for **12f**; (c) 1. TFA, dry DCM, rt, 2.5 h, 93%; 2. HCOONH<sub>4</sub> (c = 0.1 mol dm<sup>-3</sup>).

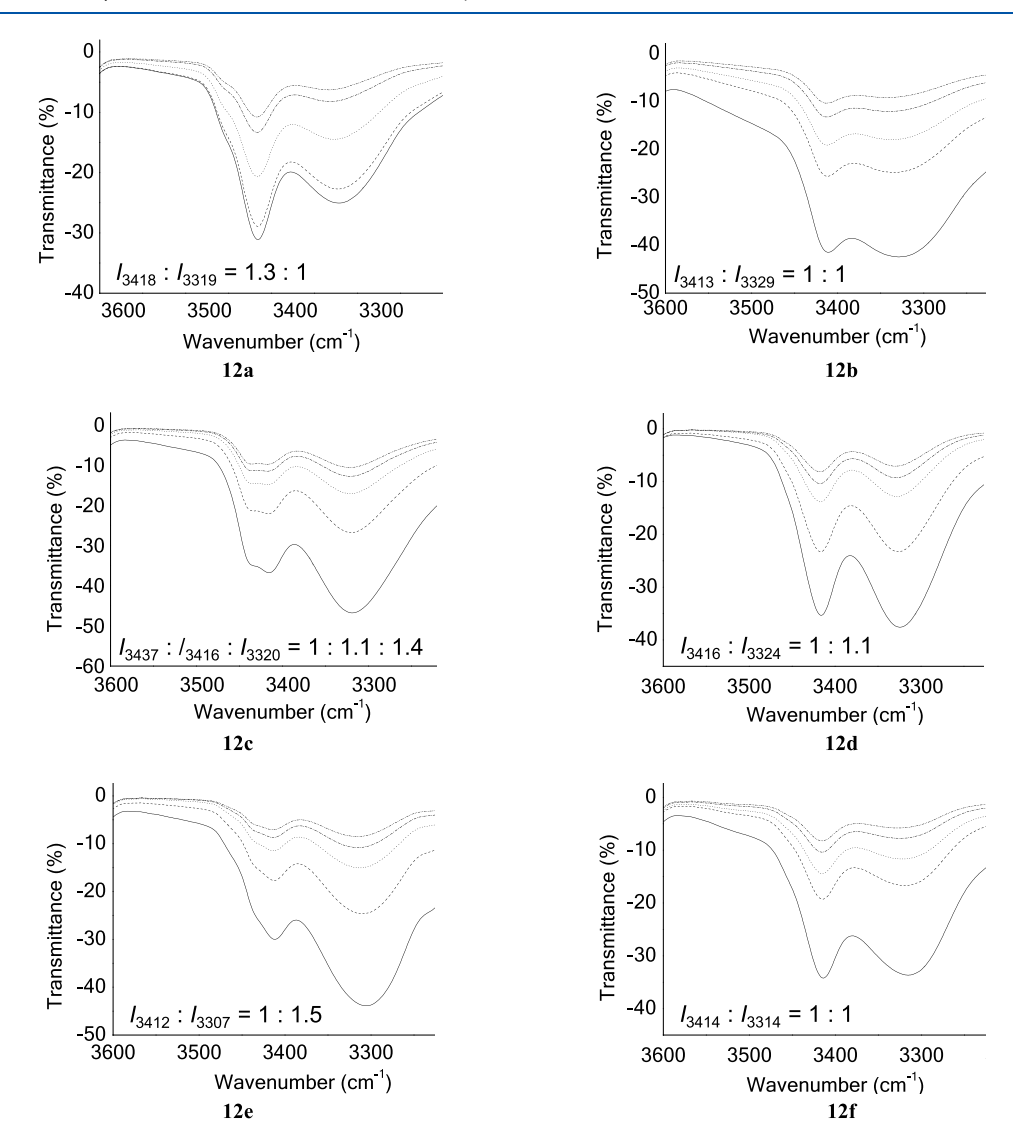


Figure 3. NH stretching vibrations in IR spectra of conjugates 12a-f in CHCl<sub>3</sub> (—)  $c = 5 \times 10^{-2}$  M, (- · -)  $c = 2.5 \times 10^{-2}$  M, (· · ·)  $c = 1.25 \times 10^{-2}$  M, (- · · -)  $c = 6.13 \times 10^{-3}$  M, (- · · -)  $c = 3 \times 10^{-3}$  M, and the ratios of the free and associated NH bands.

12f upon dilution suggests that these peptides partially form intermolecular hydrogen bonds. Conversely, conjugates 12b, 12d and 12e maintain intramolecular hydrogen bonds under the same conditions (Figure 3). The carbonyl stretching vibrations in the 1800–1600 cm<sup>-1</sup> range remained unchanged upon dilution [Supporting Information, Figures S49 (12a), S68 (12b), S86 (12c), S107 (12d), S123 (12e) and S140 (12f)].

Next, we investigated the impact of temperature on the hydrogen-bonding patterns of the peptides studied. 47,48 Temperature-dependent IR spectroscopy was performed in CHCl<sub>3</sub> at 293 K and during gradual heating to 333 K (Figure 4). No significant change in the ratio of free to hydrogen-bonded NH stretching bands was observed for conjugate 12b, indicating the presence of relatively strong and thermally stable intramolecular hydrogen bonds. In contrast, the hydrogen-

bonding patterns of conjugates 12a and 12c-f were found to be temperature-sensitive. In particular, the intensity of the hydrogen-bonded NH bands (3307–3329 cm<sup>-1</sup>) decreased with increasing temperature, while the intensity of the free NH bands (3412–3437 cm<sup>-1</sup>) increased by up to 20%.

Beyond structure determination, NMR spectroscopy serves as a crucial technique to characterize peptide folding pathways influenced by intramolecular hydrogen bonding, facilitating the identification of bioactive conformers associated with pharmacophoric properties and drug-like behavior. To enable the assignment of individual proton resonances and elucidate hydrogen bonding motifs in peptides 12a–f, a detailed NMR analysis was undertaken (<sup>1</sup>H, <sup>13</sup>C, <sup>1</sup>H–<sup>1</sup>H COSY, <sup>1</sup>H–<sup>1</sup>H NOESY, <sup>1</sup>H–<sup>13</sup>C HMQC, and <sup>1</sup>H–<sup>13</sup>C HMBC). [For the full NMR characterization, please refer to the Supporting Information: Figures S50–S62 (12a), S69–S80 (12b), S87–

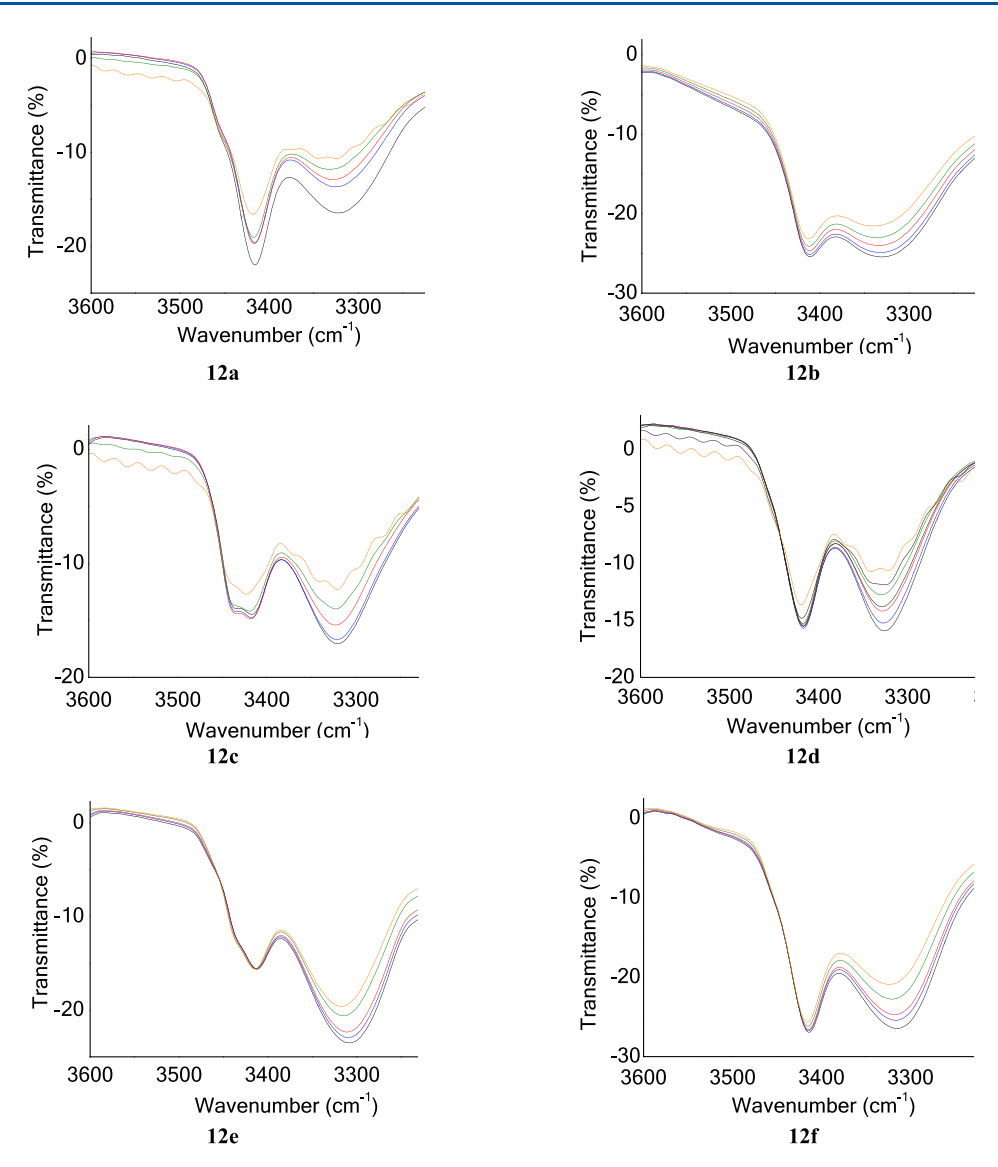


Figure 4. NH stretching vibrations in the temperature-dependent IR spectra of conjugates 12a-f in CHCl<sub>3</sub> ( $c = 5 \times 10^{-2}$  M); (black —) 293 K, (blue —) 303 K, (red —) 313 K, (green —) 323 K, (yellow —) 333 K.

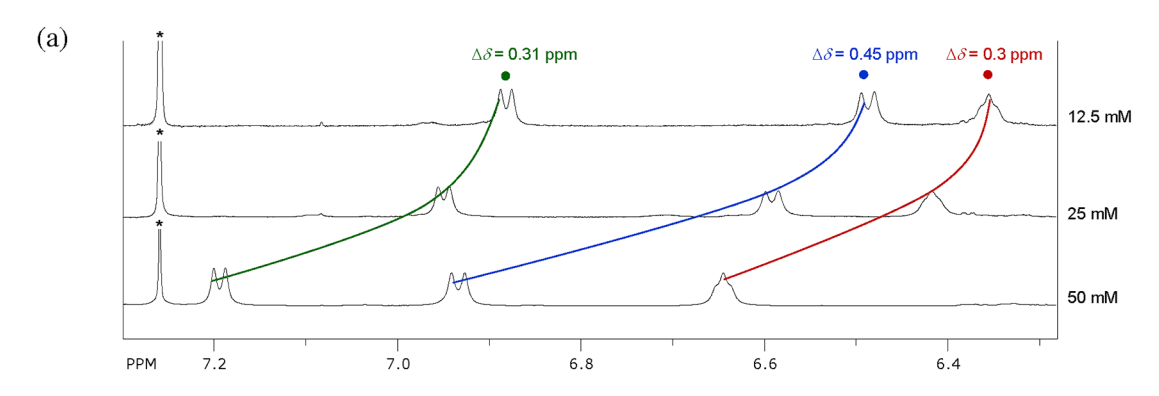
S101 (12c), S108-S117 (12d), S124-S134 (12e) and S141-S154 (12f)].

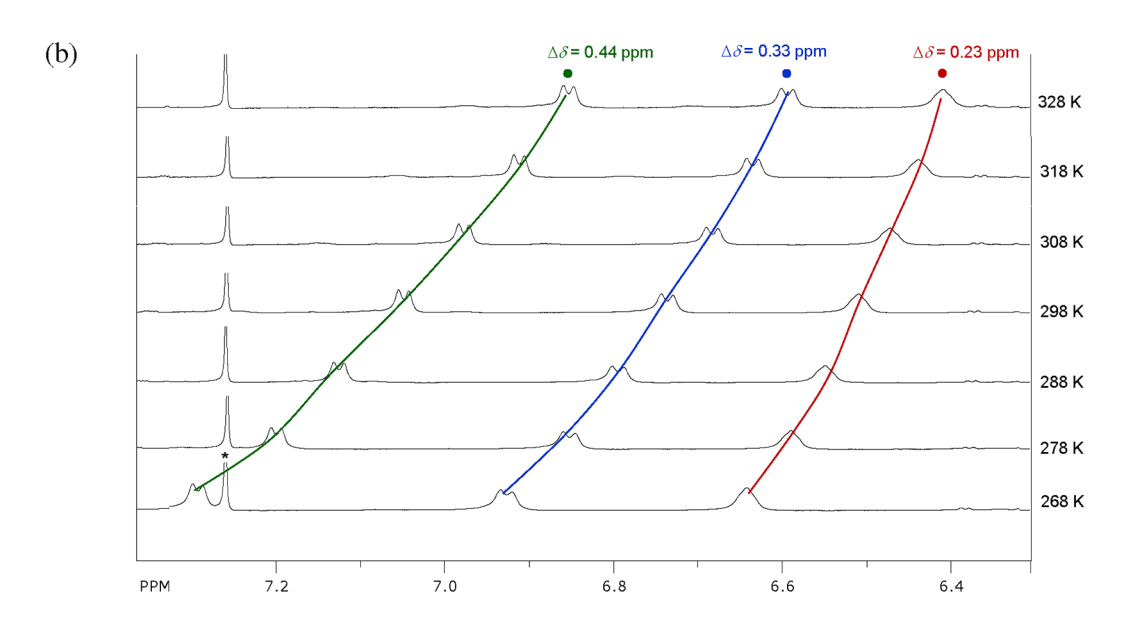
Because the protons involved in hydrogen bonds experience a deshielding effect, their signals in the nonpolar CDCl<sub>3</sub> shift downfield ( $\delta \geq 7$  ppm), <sup>50,51</sup> and the chemical shift values increase with the strength of the hydrogen bonds. Thus, only the NH<sub>Fn</sub> proton in peptide **12e**, which has the highest chemical shift ( $\delta \sim 8.6$  ppm), is involved in stronger hydrogen bonding, while the more upfield shifted resonances of the NH<sub>Gly</sub>, NH<sub>Val</sub>, and NH<sub>Glu</sub> protons ( $\delta \sim 6.7$ –7.6 ppm) in the peptides studied indicate weaker hydrogen bonding capabilities [Figures S50 (**12a**), S69 (**12b**), S87 (**12c**), S108 (**12d**), S124 (**12e**) and S141 (**12f**) and Table S1 in Supporting Information]. These findings corroborate prior conclusions that that bulky side chains interfere with hydrogen bonding interactions essential for maintaining conformational stability. <sup>17,52</sup>

To further elucidate the conformational properties of peptides 12a-f, we investigated the changes in their NH chemical shifts in response to variations in concentration, temperature, and solvent environment. (For the most bio-

logically active conjugate 12b, the results of the concentration-, temperature and DMSO-dependent chemical shifts are shown in Figure 5, while the corresponding results for the other peptides tested are shown in the Supporting Information).

Of the peptides 12a-f tested, only the IR spectra of peptides 12a, 12c and 12f showed a slight dependence on concentration (Figure 3), indicating minimal intermolecular aggregation. Therefore, a significant upfield shift of the NH signals at a dilution of up to 50-fold was not expected.<sup>53</sup> The observed smaller changes in the chemical shifts ( $\Delta \delta \sim 0.1-0.5$ ) of NH protons from 12a-f upon dilution thus corroborate the prevalence of intramolecularly hydrogen bonded states. The broad and coalesced amide peaks in conjugate 12c are due to the adoption of multiple conformations, 54 as shown by IR data. Due to coalescence at room temperature, the individual resonances for the NH proton could not be distinguished, and the observed variations in the chemical shift are presented as an average value for all analyzed protons [Figure 5a for 12b, S65 (12a), S83 (12b), S104 (12c), S120 (12d), S137 (12e) and S157 (12f) and Table S1 in Supporting Information].





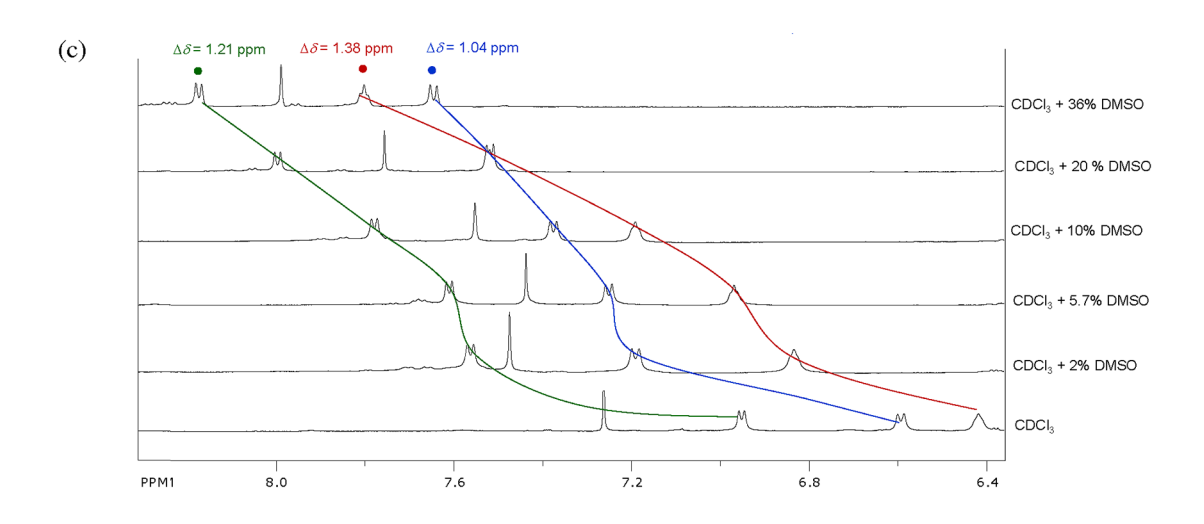


Figure 5. (a) Changes in chemical shifts ( $\Delta\delta$ ) of NH protons of conjugates 12a-f (a) in CDCl<sub>3</sub> from  $c = 5 \times 10^{-2}$  M to  $c = 1.25 \times 10^{-2}$  M, (b) in CDCl<sub>3</sub> ( $c = 1 \times 10^{-3}$  M) from 268 to 328 K, (c) at increasing concentrations of  $d_6$ -DMSO in CDCl<sub>3</sub> (c = 25 mM, 298 K).

The stability of the intramolecular hydrogen-bonded structures was assessed by monitoring the temperature-dependent chemical shift changes of the amide protons between 258 and 328 K; smaller shifts ( $\Delta\delta$ ) implied higher stability of the hydrogen-bonded conformations. Thus, the upfield shift of the NH protons observed with increasing temperature suggests involvement of 12a-f in more dynamic or less conformationally constrained hydrogen-bonding interactions [Figure 5b for 12b, S66 (12a), S84 (12b), S105 (12c), S121 (12d), S138 (12e) and S158 (12f) and Table S2 in Supporting Information].

Interestingly, the intramolecular rotation and the conformational transitions become more pronounced at 328 K and the amide protons of 12c show distinct sharp signals, indicating a consistent molecular conformation in dynamic equilibrium. With decreasing temperature, however, the signals become increasingly broader and even split into multiple peaks at 268 K (Figure S105 in Supporting Information). These observations indicate that the molecules exist in several different conformations that interconvert very slowly at lower temperatures. 54

The temperature dependence of amide proton chemical shifts, quantified as temperature coefficients  $(\Delta \delta / \Delta T)$ , provides valuable insights into hydrogen bonding interactions within peptides. Low  $\Delta\delta/\Delta T$  values (~ 2–3 ppb K<sup>-1</sup>) indicates protons that are either shielded or exposed to solvent (CDCl<sub>3</sub>). Therefore, these small shifts are of limited use in delineating specific hydrogen bonding motifs. In contrast, larger temperature coefficients are consistently observed for NH protons that are initially involved in hydrogen bonding but become solvent-accessible upon thermal perturbation, likely due to disruption of intra- or intermolecular hydrogen bonds.<sup>57–60</sup> In this study, all amide protons, with the exception of the NH<sub>Val</sub> of 12d, exhibited  $\delta/\Delta T$  values in the range of -3.8 to -10.3 ppb K<sup>-1</sup> (Table S2 in Supporting Information). Remarkably, the corresponding IR stretching frequencies and NMR chemical shifts were largely insensitive to concentration, further supporting the presence of intramolecular hydrogen bonds stabilizing these conformations.

To assess the involvement of peptides 12a–f in weak hydrogen bonding, we investigated the solvent dependence of their NH chemical shifts. The strong hydrogen-bonding solvent DMSO is known to effectively solvate the accessible NH protons in conformationally flexible peptides. S3,61–63 The significant downfield shifts ( $\Delta\delta\sim0.7-1.4$  ppm) observed with the addition of DMSO indicate that exposed NH protons are solvated, consistent with their participation in weak hydrogen bonds that are readily disrupted by competitive solvation (Figure 5c for 12b and S67 (12a), S85 (12b), S106 (12c), S122 (12d), S139 (12e) and S159 (12f) in the Supporting Information).

The previously reported ferrocene-containing peptides were involved in strong intramolecular hydrogen bonds and NOESY analysis suggested their folding into stable turn- and/or  $\beta$ -sheet-like structures. <sup>12,13,62</sup> Considering the number and position of the hydrogen bond donating and accepting sites, we searched for long-range NOE interactions between amide protons and protons distant in the primary sequence of conjugates 12a-f, which would argue for the presence of intramolecular hydrogen bonds. However, the targeted NOE cross-peaks were not observed, which is most likely due to the presence of flexible conformations formed by weak hydrogen bonds.

**2.3. Biological Evaluation.** Desmuramylpeptide derivatives based on the L-Ala-D-isoGln and L-Ala-D-Glu dipeptides or Gly-L-Val-D-Glu tripeptide core with various aromatic moieties have shown NOD2 stimulatory activities in the low nanomolar range as reported in the literature. $^{31-34}$  In the cited studies, the most promising structures were obtained by further modification of the aromatic moiety with lipophilic units<sup>31</sup> such as fatty acids, cholesterol and adamantane, which were not only beneficial for agonism but also improved their adjuvant activity and stability in vivo. In an in vitro assay, both the binding affinity of the ligand and the permeability of the cell membrane, for which the lipophilicity of the ligand is essential, play a role. To that end, we wanted to explore the ferrocene scaffold as a new aromatic motif acting as a surrogate for MurNAc. Thus, mono- and disubstituted ferrocenes were incorporated into the L-Ala-D-isoGln dipeptide and Gly-L-Val-D-Glu tripeptide, with disubstituted ferrocenes additionally decorated with various lipophilic moieties such as benzyl ether, tert-butoxycarbonyl or acetyl.

To determine the NOD2 agonistic potential of the ferrocene-based desmuramylpeptides at the cellular level, we used the validated and commercially available HEK-Blue NOD2 cell line reporter assay. HEK-Blue hNOD2 cells were first treated for 18 h with ferrocene derivatives at 10  $\mu$ M. The NF- $\kappa$ B transcriptional activity measured was normalized to that of the vehicle treated (0.1% DMSO) control HEK-Blue hNOD2 cells (Figures 6 and S184 in Supporting Information).

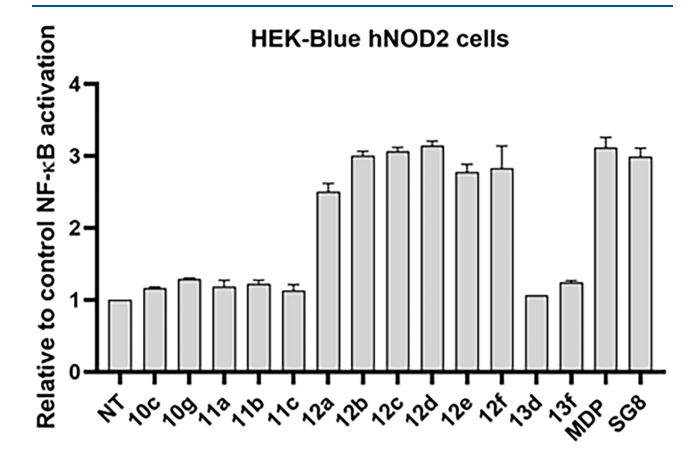


**Figure 6.** NOD2 agonistic activities of ferrocene-featuring desmuramylpeptides. HEK-Blue hNOD2 cells were treated with **MDP** as the positive control, **SG8** (10  $\mu$ M) as the reference compound, and ferrocene-featuring desmuramylpeptides (10  $\mu$ M) for 18 h. The SEAP activities are shown relative to that of the untreated control (0.1% DMSO; NT). Data are means  $\pm$  SEM of three independent experiments.

None of the ferrocene-incorporating desmuramylpeptides were cytotoxic toward the HEK-Blue hNOD2 cells at the highest tested concentration (20  $\mu$ M), as determined by the (3-(4,5-dimethylthiazol-2-yl)-5-(3-carboxymethoxyphenyl)-2-(4-sulfophenyl)-2H-tetrazolium) (i.e., MTS) cell viability assay (Figure 7).

First, a ferrocene moiety was introduced as a surrogate for *N*-acetylmuramic acid into a series of L-Ala-D-isoGln dipeptides, yielding compounds 10c/g, 11a-c, and 13d/f. Second, replacement of the *trans*-ferruloyl moiety in hit compound SG8<sup>34</sup> resulted in desmuramylpeptides 12a-f. While all ferrocene-decorated L-Ala-D-isoGln derivatives were

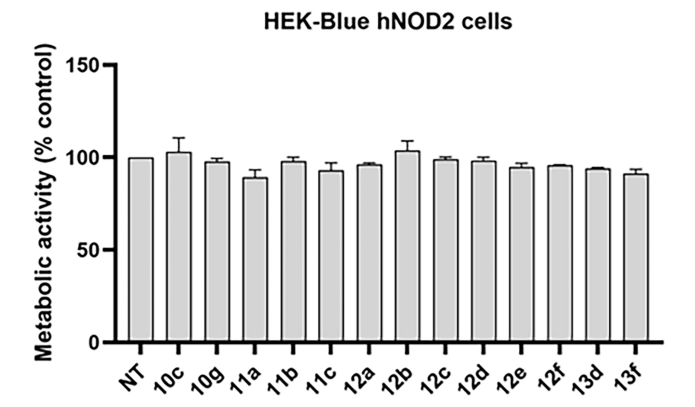


Figure 7. Metabolic activities of HEK-Blue hNOD2 were measured after 18 h treatment with ferrocene-featuring desmuramylpeptides (20  $\mu$ M). Data are shown relative to untreated control (0.1% DMSO; NT). Data are means  $\pm$  SEM of two independent experiments.

almost completely devoid of NOD2 agonist activity, the compounds based on the Gly–L-Val–D-Glu tripeptide scaffold (12a–12f) exhibited significant activity at 10  $\mu$ M, with fold inductions ranging from 2.50 to 3.14 – comparable to MDP (3.12-fold) and SG8 (2.99-fold). These compounds were therefore selected for further dose–response analysis. Their

 $EC_{50}$  values were determined and compared to those of MDP and SG8 (Table 1).

The most potent NOD2 agonist was the monosubstituted conjugate  $Fn-CH_2-CO-Gly-L-Val-D-Glu(OEt)_2$  (12b,  $EC_{50}=44.1$  nM), which contains a flexible methylene linker tethering the ferrocene scaffold to the tripeptide core; while it was approximately twice as potent as MDP ( $EC_{50}=80.5$  nM), it proved somewhat inferior to SG8 ( $EC_{50}=16.7$  nM). The removal of the methylene linker resulted in a marked decrease in activity as evidenced by its homologue  $Fn-CO-Gly-L-Val-D-Glu(OEt)_2$  (12a,  $EC_{50}=563.3$  nM), suggesting an important role of the methylene group for NOD2 agonistic activity. It should also be noted that its dipeptide counterpart  $Fn-CH_2-CO-L-Ala-D-isoGln-OH$  (11b), which carries the same flexible methylene linker spanning the ferrocene scaffold and the dipeptide core as seen with 12b, showed weak NOD2 agonist activity at 10  $\mu$ M.

Disubstitution of the ferrocene scaffold had no significant impact on agonist activity compared to the monosubstituted analog Fn–CO–Gly–L-Val–D-Glu(OEt)<sub>2</sub> (12a). This comparison seemed most relevant given that all disubstituted ferrocene analogs featured the same linkage type to the tripeptide core. Among the disubstituted derivatives, Boc–NH–Fn–CO–Gly–L-Val–D-Glu(OEt)<sub>2</sub> (12c) featuring an additional *N*-Boc group on the ferrocene scaffold showed the

Table 1. In Vitro NOD2 Agonistic Activities of 10c/g, 11a-c, 12a-f and 13d/f on HEK-Blue hNOD2 Cells Expressed as EC<sub>50</sub> Values and Compared to MDP and SG8 as Reference Compounds<sup>a</sup>

$\begin{array}{c c} & & & \\ & & & \\ R^1 & & & \\ & & & \\ H & & \\ & & & \\ & & \\ H_2 N & \\ \end{array} \\ \begin{array}{c} & \\ \\ \\ \\ \\ \\ \\ \end{array} \\ \begin{array}{c} \\ \\ \\ \\ \\ \\ \\ \\ \end{array} \\ \begin{array}{c} \\ \\ \\ \\ \\ \\ \\ \\ \end{array} \\ \begin{array}{c} \\ \\ \\ \\ \\ \\ \\ \\ \end{array} \\ \begin{array}{c} \\ \\ \\ \\ \\ \\ \\ \\ \end{array} \\ \begin{array}{c} \\ \\ \\ \\ \\ \\ \\ \\ \end{array} \\ \begin{array}{c} \\ \\ \\ \\ \\ \\ \\ \\ \\ \\ \end{array} \\ \begin{array}{c} \\ \\ \\ \\ \\ \\ \\ \\ \\ \\ \\ \end{array} \\ \begin{array}{c} \\ \\ \\ \\ \\ \\ \\ \\ \\ \\ \\ \end{array} \\ \begin{array}{c} \\ \\ \\ \\ \\ \\ \\ \\ \\ \\ \\ \\ \end{array} \\ \begin{array}{c} \\ \\ \\ \\ \\ \\ \\ \\ \\ \\ \\ \\ \\ \\ \\ \\ \\ \\ \\$				R H O H O OEt		
compound	R <sup>1</sup>	$\mathbb{R}^2$	EC <sub>50</sub> /nM	compound	R	EC <sub>50</sub> /nM
10c	NHBoc Fe	CH <sub>2</sub> Ph	n.a.	12a	-Fe	563.3
10g	NH <sub>2</sub>	Bn	n.a.	12b	-re-	44.1
11a		Н	n.a.	12c	NHBoc Fe	252.6
11b	-re-	Н	n.a.	12d	CH <sub>2</sub> OBn	718.5
11c	NHBoc Fe	Н	n.a.	12e	NHAc Fe	2636.3
13d	CH <sub>2</sub> OBn	<i>t</i> Bu	n.a.	12f	CH <sub>2</sub> OH	898.7
13f	CH <sub>2</sub> OH	<i>t</i> Bu	n.a.	SG8	MeO HO	16.7
MDP	HO NHAC OH	н	80.5			

an.a. = not active.

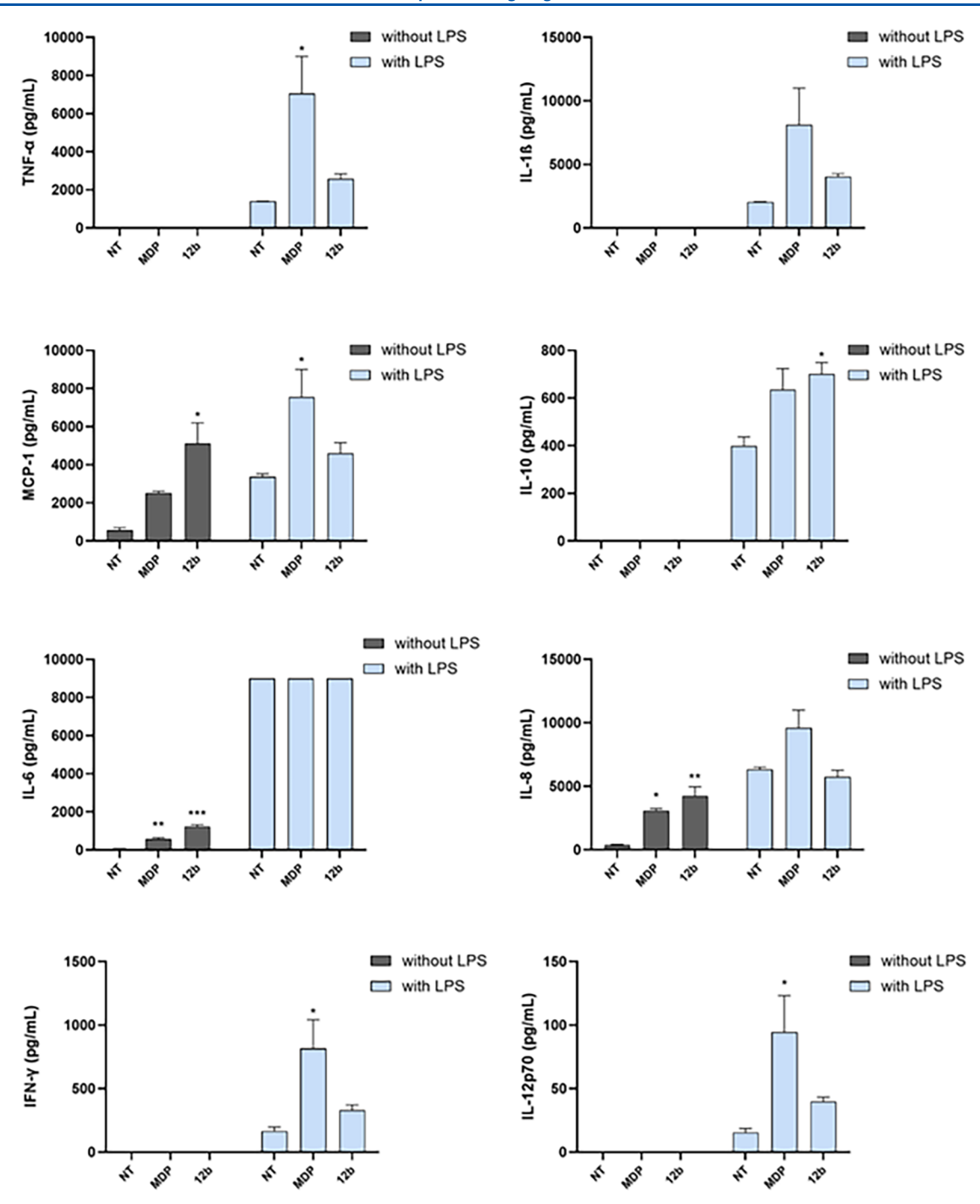


Figure 8. Effects of the MDP and desmuramylepetide 12b on cytokine release from human PBMCs. Cytokine and chemokine concentrations were measured after 18 h stimulation with MDP (1  $\mu$ M) or 12b (1  $\mu$ M) in the absence or presence of LPS (20 ng/mL). Data are means  $\pm$  SEM of 2 independent experiments. Statistical significance was determined using one-way ANOVA with posthoc Dunnett's test; \* $p \le 0.05$ , \*\* $p \le 0.01$ , \*\*\* $p \le 0.001$  versus control (NT).

highest potency (EC<sub>50</sub> = 252.6 nM); in fact, its NOD2 activity was increased by a factor of 2. Weak agonist activities (observed at 10  $\mu$ M) of its Boc-protected dipeptide counterparts Boc-NH-Fn-CO-L-Ala-D-isoGln(OBn) (10c) and Boc-NH-Fn-CO-L-Ala-D-isoGln-OH (11c), highlights the decisive influence of the tripeptide motif on the agonist potential of its conjugates. Replacement of the *N*-Boc group with the bulkier benzyl ether group in Ph-CH<sub>2</sub>-O-CH<sub>2</sub>-Fn-CO-Gly-L-Val-D-Glu(OEt)<sub>2</sub> (12d) or a smaller acetamide group in Ac-NH-Fn-CO-Gly-L-Val-D-Glu(OEt)<sub>2</sub>

(12e) further decreased the NOD2 agonist activity (EC $_{50}$  = 718.5 and 2636.3 nM, respectively). Moreover, the benzyl deprotection of 12d that led to HO–CH $_2$ –Fn–CO–Gly–L-Val–D-Glu(OEt) $_2$  (12f) had no impact on NOD2 agonist activity (EC $_{50}$  = 898.7 nM).

The immunostimulatory effects of the best performing ferrocene desmuramylpeptide 12b and the reference compound MDP were evaluated using human primary peripheral blood mononuclear cells (PBMCs). This heterogeneous population of immune cells provides a physiologically relevant

system to study the activity of NOD2 agonists, given the presence of various NOD2-interacting and downstream signaling proteins. To assess the cytokine and chemokine profiles elicited by NOD2 activation, we initially employed the LEGENDplex Human Essential Immune Response Panel. Furthermore, considering that NOD2 activation serves as a key amplification signal for Toll-like receptor (TLR)-induced inflammatory responses, we also evaluated cytokine and chemokine secretion following costimulation with lipopoly-saccharide (LPS), a well-characterized TLR4 agonist.<sup>64,65</sup> Figure 8 presents the effects of 12b and MDP (both at 1  $\mu$ M) on the secretion of TNF- $\alpha$ , IL-1 $\beta$ , MCP-1, IL-10, IL-6, IL-8, IFN-γ, and IL-12p70, both alone and in combination with LPS (20 ng/mL). Overnight stimulation of PBMCs with 12b resulted in marked increases in MCP-1, IL-6, and IL-8 levels, exceeding those induced by MDP. LPS stimulation alone significantly elevated the secretion of all measured cytokines; this response was further amplified when combined with either 12b or MDP in most cases. Notably, IL-6 production did not increase further upon costimulation, suggesting a plateau or saturation in IL-6 secretion under these conditions. Relative to LPS alone, costimulation with MDP statistically significantly enhanced the production of TNF- $\alpha$ , MCP-1, IFN- $\gamma$ , and IL-12p70. Compound 12b elicited a similar cytokine and chemokine response profile; however, only IL-10 levels matched those induced by the MDP/LPS combination, while the other cytokines were produced at comparatively lower levels. In general, these findings are consistent with previously reported synergistic signal amplification between NOD2 and TLR4 pathways.<sup>64-</sup>

#### 3. CONCLUSIONS

In this study, we successfully designed and synthesized a series of novel desmuramylpeptides as NOD2 agonists by integrating ferrocene scaffolds with dipeptide and tripeptide cores. The conformational analysis showed that the peptides studied adopt relatively flexible structural arrangements. Of the six peptides analyzed (12a-f), IR spectroscopy revealed predominant hydrogen bonding only in conjugates 12c and 12e. The upfield shifts of the NH protons in these conjugates support the IR data and confirm the absence of significant hydrogen bonding. In addition, the NH proton chemical shifts showed pronounced sensitivity to temperature and DMSO, further indicating conformational flexibility likely due to weak hydrogen-bonding interactions.

Structure-activity relationship analyses identified compound 12b as the most potent NOD2 agonist, exhibiting low nanomolar activity and outperforming the reference compound MDP. The enhanced potency of 12b was attributed to the presence of a flexible methylene linker connecting the ferrocene moiety to the tripeptide backbone, highlighting the importance of structural flexibility for optimal receptor activation. Further immunological evaluation using human primary PBMCs confirmed the ability of 12b to induce a proinflammatory cytokine and chemokine response, particularly in combination with LPS, a TLR4 agonist. These findings reinforce the functional relevance of 12b in a physiologically representative immune context and underscore the synergistic interplay between NOD2 and TLR4 pathways. Together, these results position ferrocene-incorporating desmuramylpeptide 12b as a promising lead compound for further development as a NOD2-targeted immunomodulator or vaccine adjuvant.

#### 4. EXPERIMENTAL SECTION

**4.1. General Methods.** The ferrocene precursors (1, B and 4) were synthesized following the previously reported protocols. 68,69 The dipeptide Boc-L-Ala-D-isoGln(OBn), which was used for the synthesis of compound 7, and D-Glu-OH, which was used for the preparation of compounds 8 and 9, were purchased from Bachem (Switzerland). All other chemicals and solvents were purchased from Sigma-Aldrich Corp. (Germany). The organic solvents were purified and/or dried using standard laboratory techniques before use. Thin layer chromatography (TLC) was performed on Fluka silica gel (60 F254) plates (0.25 mm). Column chromatography was conducted using Merck silica gel 60 (size 70-230 mesh ASTM). The compound purity was determined by high-performance liquid chromatography (HPLC) with the results documented in the Supporting Information [Figures S12 (10c), S23 (10g), S33 (11a), S43 (11b), S48 (11c), S64 (12a), S82 (12b), S103 (12c), S119 (12d), S136 (12e), S156 (12f), S172 (13d) and S183 (13f)]. The HPLC analyses were performed using an Agilent Technologies 1200 series instrument, equipped with a binary pump, a degasser, an autosampler, and a diode array detector (DAD). The mobile phase consisted of Milli-Q water containing 0.1% formic acid (solvent A), and HPLC-grade methanol (solvent B), supplied by J. T. Baker. Chromatographic separation was performed using a Zorbax XDB-C18 column (4.6  $\times$  75 mm, 3.5  $\mu$ m). The gradient elution program was as follows: 40% B at 0 min, increase to 100% B at 12 min, return to 40% B in 15.1 min, and hold at 40% B until 20 min. The flow rate was maintained at 0.5 mL/min, and the injection volume was 5  $\mu$ L. Mass spectrometric analysis was conducted on an Agilent 6410 triple quadrupole mass spectrometer. High-resolution mass spectrometry (HRMS) was carried out using an Agilent 6546 LC/Q-TOF instrument coupled to a 1290 Infinity II UHPLC. Infrared (IR) spectra were acquired from CHCl<sub>3</sub> solutions between NaCl windows using a Spectrum Two FTIR spectrometer (PerkinElmer). The absorption bands were labeled as strong (s), medium (m), weak (w), broad (br), or shoulder (sh). The <sup>1</sup>H and <sup>13</sup>C NMR spectra were recorded using the Bruker AV- III HD spectrometer at 400 MHz (1H) and 100 MHz (13C). The NMR data were analyzed using SpinWorks and Bruker TopSpin processing software. The chemical shifts  $(\delta, ppm)$  were referenced to the residual solvent peaks: CDCl<sub>3</sub> ( ${}^{1}$ H: 7.26 ppm;  ${}^{13}$ C: 77.16 ppm) CD<sub>3</sub>OD ( ${}^{1}$ H: 3.31 ppm;  ${}^{13}$ C: 49.0 ppm), DMSO- $d_6$  ( ${}^{1}$ H: 2.50 ppm;  ${}^{13}$ C: 39.5 ppm). The signals assignments were confirmed by two-dimensional NMR techniques, including <sup>1</sup>H-<sup>1</sup>H COSY (Correlation Spectroscopy) and <sup>1</sup>H-<sup>1</sup>H NOESY (Nuclear Overhauser Effect Spectroscopy). Double resonance experiments were performed using the Bruker Avance spectrometer at the Ruđer Bošković Institute. NMR titrations were conducted by incremental addition (10 µL) of DMSO to CDCl<sub>3</sub> solutions of the goal peptides ( $c = 2.5 \times 10^{-2}$  M), and spectra were recorded after each addition. The titration was completed when no further changes in chemical shift of the amide protons were observed upon subsequent addition of DMSO- $d_6$ . As DMSO was used as the solvent for the biological evaluation, a  $^1\mathrm{H}$  NMR stability study was conducted to assess the stability of the tested compounds upon dissolution in DMSO and after 18 h, corresponding to the incubation time in biological assays. As shown in Figure S185 in the Supporting Information, no significant changes in the chemical shifts were observed over this period, indicating that conjugates 12a-f remained stable in DMSO under the tested conditions.

**4.2.** Synthesis of Ferrocene Carboxylic Acids (C – D). 4.2.1. Methyl (1'-hydroxymethyl)ferrocene-1-carboxylate (2). To a solution of compound 1 (100 mg, 0.35 mmol) in dry DCM (5 mL) SOCl<sub>2</sub> was added (78.3  $\mu$ L, 1.08 mmol), and the mixture was stirred for 30 min at room temperature. Pyridine was added next (83.9  $\mu$ L, 1.05 mmol), and the solution was mixed under reflux for 2 h. It was monitored by TLC (DCM/EtOAc, 5:1). After reaction completion, the mixture was evaporated *in vacuo* and the crude product triturated with dry Et<sub>2</sub>O. Red-orange organic layers were collected and evaporated. The crude product was used in the next step without further purification. To a suspension of a crude acyl halide (123 mg, 0.38 mmol) and NaBH<sub>4</sub> (43.1 mg, 1.14 mmol) in dry THF (4 mL)

MeOH was added dropwise (0.96 mL, 0.024 mmol) within 1 h. The mixture was stirred at room temperature for 1.5 h. It was monitored by TLC (DCM/EtOAc, 5:1). Brine (30 mL) was added after reaction completion, and the mixture was extracted with EtOAc (3 × 30 mL). Organic layers were dried over anhydrous Na<sub>2</sub>SO<sub>4</sub>, filtered off and the solvent was evaporated *in vacuo*. Crude product was purified by column chromatography (DCM/EtOAc, 5:1). Compound **2** was obtained as orange oil (67.6 mg, 80%).  $R_f$  = 0.20 (DCM/EtOAc, 5:1). <sup>1</sup>H NMR (CDCl<sub>3</sub>)  $\delta$ /ppm: 4.81 (t, 2H, J = 1.9 Hz, 2 CH-Fn); 4.44 (t, 2H, J = 2.0 Hz, 2 CH-Fn); 4.35 (s, 2H, CH<sub>2</sub>O); 4.27 (t, 2H, J = 1.8 Hz, 2 CH-Fn); 4.22 (t, 2H, J = 1.9 Hz, 2 CH-Fn); 3.85 (s, 3H, CH<sub>3</sub>O). <sup>13</sup>C NMR (CDCl<sub>3</sub>)  $\delta$ /ppm: 172.8 (C=O); 90.6 (C-Fn); 71.7 (CH-Fn); 71.3 (C-Fn); 70.5, 69.4, 68.7 (CH-Fn); 60.2 (CH<sub>2</sub>O); 51.9 (CH<sub>3</sub>O). ESI-MS: m/z 257.1 [M-OH]<sup>+</sup>.

4.2.2. Methyl [(1'-benzyloxy)methyl]ferrocene-1-carboxylate (3). To a suspension of 2 (40 mg, 0.14 mmol) and Ag<sub>2</sub>O (193.4 mg, 0.83 mmol) in dry DCM (5 mL) benzyl bromide was added (83  $\mu$ L, 0.69 mmol) and the mixture was stirred for 6 days in the dark at room temperature. It was monitored by TLC (DCM/EtOAc, 5:1). After reaction completion, the precipitate was filtered off and washed with DCM. The organic solution was evaporated in vacuo. Crude product was purified by column chromatography (DCM/EtOAc, 5:1). Compound 3 was obtained as dark brown oil (38.7 mg, 76%).  $R_{\rm f}$  = 0.82 (DCM/EtOAc, 5:1). <sup>1</sup>H NMR (CDCl<sub>3</sub>)  $\delta$ /ppm: 7.37–7.30 (m, 5H, Ph); 4.77 (t, 2H, J = 2.0 Hz, 2 CH-Fn); 4.53 (s, 2H, CH<sub>2</sub>Ph); 4.38 (t, 2H, J = 1.9 Hz, 2 CH-Fn); 4.29-4.28 (m, 4H, 2 CH-Fn,  $CH_2O$ ); 4.23 (t, 2H, J = 1.8 Hz, 2 CH-Fn); 3.77 (s, 3H,  $CH_3O$ ). <sup>13</sup>C NMR (CDCl<sub>3</sub>)  $\delta$ /ppm: 171.8 (C=O); 138.3 (C-Ph); 128.4, 127.7, 127.6 (CH-Ph); 84.8 (C-Fn); 72.1 (C-Fn); 72.0 (CH<sub>2</sub>Ph); 71.6, 70.9, 70.6, 70.2 (CH-Fn); 67.4 (CH<sub>2</sub>O); 51.5 (CH<sub>3</sub>O). ESI-MS: *m/z* 387.1  $[M + Na]^+$ 

4.2.3. 1'-(Methoxycarbonyl)ferrocen-1-ylammonium trifluoroacetate (5). To a solution of 4 (50 mg, 0.14 mmol) in dry DCM (3 mL) TFA was added (0.2 mL, 2.6 mmol). The reaction mixture was stirred at room temperature for 1 h. It was monitored by TLC (DCM/MeOH, 12:1). After reaction completion, the mixture was evaporated in vacuo and the crude product purified by column chromatography (DCM/MeOH, 12:1): Compound 5 was obtained as dark brown oil (35 mg, 68%).  $R_{\rm f}$  = 0.64 (DCM/MeOH, 12:1).  $^{\rm 1}{\rm H}$  NMR (CDCl<sub>3</sub>)  $\delta$ /ppm: 4.78 (s, 2H, 2 CH-Fn); 4.37 (s, 2H, 2 CH-Fn); 4.00 (s, 2H, 2 CH-Fn); 3.90 (s, 2H, 2 CH-Fn); 3.82 (s, 3H, CH<sub>3</sub>O); 2.83 (s, 2H, NH<sub>2</sub>).  $^{\rm 13}{\rm C}$  NMR (CDCl<sub>3</sub>)  $\delta$ /ppm: 171.5 (C=O); 106.9 (C-Fn); 72.4 (C-Fn); 71.7, 70.9, 70.6, 65.1, 59.3 (CH-Fn); 51.5 (CH<sub>3</sub>O). ESI-MS: m/z 259.1 [M]<sup>+</sup>.

4.2.4. Methyl 1'-(ethanoylamido)ferrocene-1-carboxylate (6). To a solution of 5 (120 mg, 0.32 mmol) in dry DCM (4 mL) acetyl chloride (46  $\mu$ L, 0.63 mmol) and pyridine (52  $\mu$ L, 0.64 mmol) were added. The reaction mixture was stirred at room temperature for 2 h. It was monitored by TLC (DCM/MeOH, 12:1). After reaction completion, the mixture was evaporated *iv vacuo* and the crude product purified by column chromatography (DCM/MeOH, 12:1): Compound 6 was obtained as dark brown oil (73 mg, 75%).  $R_f$  = 0.65 (DCM/MeOH, 12:1). <sup>1</sup>H NMR (CDCl<sub>3</sub>)  $\delta$ /ppm: 6.88 (s, 1H, NH); 4.81 (t, 2H, J = 1.9 Hz, 2 CH-Fn); 4.61 (t, 2H, J = 1.9 Hz, 2 CH-Fn); 4.43 (t, 2H, J = 1.9 Hz, 2 CH-Fn); 4.05 (t, 2H, J = 1.9 Hz, 2 CH-Fn); 3.82 (s, 3H, CH<sub>3</sub>O); 2.10 (s, 3H, CH<sub>3</sub>-Ac). <sup>13</sup>C NMR (CDCl<sub>3</sub>)  $\delta$ /ppm: 171.7, 168.7 (2 × C=O); 94.8(C-Fn); 72.4 (C-Fn); 72.3, 71.1, 66.3, 63.5 (CH-Fn); 51.7 (CH<sub>3</sub>O); 23.9 (CH<sub>3</sub>-Ac). ESI-MS: m/z 270.1 [M-OCH<sub>3</sub>]<sup>+</sup>.

**4.3.** General Procedure for Saponification of Compounds **3**, **4 and 6**. To a suspension of either 3 or 4 or 6 (0.14 mmol) in 1,4-dioxane (1 mL) aqueous solution of NaOH (1.4 mmol, c = 1 mol dm<sup>-3</sup>) was added. The mixture was stirred for 48 h (compounds **3** and **4**) or 72 h (compound **6**) in the dark at room temperature and monitored by TLC. After reaction completion, it was evaporated *in vacuo*. The crude product was acidified to pH 2 with HCl (c = 1 mol dm<sup>-3</sup>), and the solution was extracted three times with CHCl<sub>3</sub>. Organic layers were dried over anhydrous Na<sub>2</sub>SO<sub>4</sub>, filtered off, and the solvent was evaporated *in vacuo*. Crude product was purified by

column chromatography (solvents for TLC monitoring and column chromatography for each compound are stated hereafter).

4.3.1.  $(1^7$ -tert-butyloxycarbonylamino)ferrocene-1-carboxylic acid (C). An orange oil (32 mg, 67%).  $R_f=0.10$  (DCM/EtOAc, 5:1).  $^1$ H NMR (CDCl<sub>3</sub>)  $\delta$ /ppm: 8.55 (s, 1H, NH); 4.96 (s, 2H, 2 × CH-Fn); 4.58 (s, 2H, 2 × CH-Fn); 4.42 (s, 2H, 2 × CH-Fn); 3.97 (s, 2H, 2 × CH-Fn); 1.67 (s, 9H, 3 × CH<sub>3</sub>-Boc).  $^{13}$ C NMR (CDCl<sub>3</sub>)  $\delta$ /ppm: 175.7 (C=O), 155.5 (C=O, Boc); 98.6 (C-Fn); 82.1 (C(CH<sub>3</sub>)<sub>3</sub>-Boc); 73.1 (C-Fn); 71.5, 71.3, 65.3, 60.5 (CH-Fn); 28.4 (C(CH<sub>3</sub>)<sub>3</sub>-Boc). ESI-MS: m/z 344.5 [M]<sup>-</sup>.

4.3.2. [(1'-Benzyloxy)methyl]ferrocene-1-carboxylic acid (D). Dark brown oil (47 mg, 91%).  $R_f$  = 0.10 (DCM/EtOAc, 5:1).  $^1$ H NMR (CDCl<sub>3</sub>)  $\delta$ /ppm: 7.40–7.30 (m, 5H, Ph); 4.83 (s, 2H, CH<sub>2</sub>Ph); 4.54 (s, 2H, 2 CH-Fn); 4.46 (s, 2H, 2 CH-Fn); 4.33 (s, 4H, 2 CH-Fn, CH<sub>2</sub>O); 4.28 (s, 2H, 2 CH-Fn).  $^{13}$ C NMR (CDCl<sub>3</sub>)  $\delta$ /ppm: 177.2 (C=O); 138.2 (C-Ph); 128.4, 127.8, 127.6 (CH-Ph); 85.1 (C-Fn); 72.5 (C-Fn); 72.1 (CH<sub>2</sub>Ph); 71.1, 70.5 (CH-Fn); 67.3 (CH<sub>2</sub>O). ESI-MS: m/z 373.1 [M + Na]<sup>+</sup>.

4.3.3. 1'-(Ethanoylamido)ferrocene-1-carboxylic acid (E). An orange-brown solid (47 mg, 82%).  $R_{\rm f}=0.31$  (DCM/MeOH, 12:1). mp = 157 °C (decomp.). ¹H NMR (CD<sub>3</sub>OD)  $\delta$ /ppm: 4.78 (s, 2H, 2 CH-Fn); 4.68 (s, 2H, 2 CH-Fn); 4.43 (s, 2H, 2 CH-Fn); 4.04 (s, 2H, 2 CH-Fn); 2.05 (s, 3H, CH<sub>3</sub>-Ac). ¹³C NMR (CD<sub>3</sub>OD)  $\delta$ /ppm: 173.8 (2 × C=O); 96.1 (C-Fn); 72.1, 70.8, 65.8, 62.1 (CH-Fn); 56.9 (C-Fn); 22.0 (CH<sub>3</sub>-Ac). ESI-MS: m/z 288.1 [M + H]<sup>+</sup>.

**4.4.** Synthesis of Goal Peptides 10c/g, 11a-c, 12a-f, 13d/f. 4.4.1. General Procedure for the Preparation of Peptide Derivatives 10a-c, 13d and 12a-e. To a suspension of 7, 8 or 9 (0.19 mmol) and corresponding carboxylic acid derivative (0.21 mmol) in dry DCM (4 mL) at 0 °C TEA (0.48 mmol) was added. After the addition of EDC × HCl (0.21 mmol) and HOBt (0.21 mmol) the reaction mixture was stirred at 0 °C for 1h and at room temperature for an additional 48h. It was monitored by TLC (CHCl<sub>3</sub>/MeOH, 10:1). After reaction completion, DCM (15 mL) was added and the mixture was washed with HCl (2 × 20 mL, c = 0.5 mol dm<sup>-3</sup>), NaHCO<sub>3</sub> saturated aqueous solution (20 mL) and brine (20 mL). The organic layer was dried over anhydrous Na<sub>2</sub>SO<sub>4</sub>, filtered off, and the solvent was evaporated *in vacuo*. Crude product was purified by column chromatography (CHCl<sub>3</sub>/MeOH, 10:1 for 10a-c, 12b and 13d; EtOAc/DCM, 5:1 for 12a, 12c-e).

4.4.1.1. (4R)-Benzyl 4-carbamoyl-4-[(2S)-(ferrocenoylamido)-propanoylamido]butanoate (10a). An orange-yellow oil (76 mg, 77%).  $R_f = 0.52$  (CHCl<sub>3</sub>/MeOH, 10:1). <sup>1</sup>H NMR (CDCl<sub>3</sub>)  $\delta$ /ppm: 7.97 (d, 1H, J = 7.3 Hz, NH); 7.38–7.32 (m, 5H, Ph); 7.17 (s, 1H, NH); 7.08 (s, 1H, NH); 6.66 (s, 1H, NH); 5.11 (s, 2H, CH<sub>2</sub>–Bn); 4.74–4.70 (m, 3H, 2 × CH-Fn, CHα-isoGln); 4.51–4.46 (m, 1H, CHα-Ala); 4.30–4.29 (m, 2H, 2 × CH-Fn); 4.16 (s, 5H, 5 × CH-Fn); 2.59–2.47 (m, 2H, CH<sub>2</sub>–isoGln); 2.34–2.26 (m, 1H, CH-isoGln); 2.07–1.96 (m, 1H, CH-isoGln); 1.47 (d, 3H, J = 7.0 Hz, CH<sub>3</sub>–Ala). <sup>13</sup>C NMR (CDCl<sub>3</sub>)  $\delta$ /ppm: 174.2, 174.0, 173.0, 171.6 (4 × C=O); 135.7 (C-Ph); 128.6, 128.3, 128.2 (CH-Ph); 74.6 (C-Fn); 70.9, 70.8, 69.8, 68.4 (CH-Fn); 66.6 (CH<sub>2</sub>–Bn); 58.4 (C-Fn); 52.7 (CHα-isoGln); 49.5 (CHα-Ala); 30.9, 26.8 (CH<sub>2</sub>–isoGln); 18.4 (CH<sub>3</sub>–Ala). ESI-MS: m/z 520.0 [M + H]<sup>+</sup>.

4.4.1.2. (4 R) - B e n z y I 4 - c a r b a m o y I - 4 - [(2 S) - (ferrocenylethanoylamido)propanoylamido] butanoate (10b). A brown oil (45.6 mg, 45%).  $R_{\rm f} = 0.58$  (CHCl<sub>3</sub>/MeOH, 10:1). <sup>1</sup>H NMR (CDCl<sub>3</sub>) δ/ppm: 7.43–7.36 (m, 6H, Ph, NH); 6.80 (s, 1H, NH); 6.48 (s, 1H, NH); 5.89 (s, 1H, NH); 5.13 (s, 2H, CH<sub>2</sub>–Bn); 4.45–4.34 (m, 2H, CHα-isoGln, CHα-Ala); 4.22–4.15 (m, 9H, 9 × CH-Fn); 3.33 (s, 2H, CH<sub>2</sub>–Fn); 2.53–2.47 (m, 2H, CH<sub>2</sub>–isoGln); 2.24–2.21 (m, 1H, CH-isoGln); 2.07–2.00 (m, 1H, CH-isoGln); 1.30 (s, 3H, CH<sub>3</sub>–Ala). <sup>13</sup>C NMR (CDCl<sub>3</sub>) δ/ppm: 173.5, 173.4, 172.8, 171.7 (4 × C=O); 135.6 (C-Ph); 128.6, 128.4, 128.3 (CH-Ph); 80.5 (C-Fn); 69.1, 68.9, 68.6, 68.5 (CH-Fn); 66.7 (CH<sub>2</sub>–Bn); 52.5 (CHα-isoGln); 49.5 (CHα-Ala); 37.6 (CH<sub>2</sub>–Fn); 30.6, 26.7 (CH<sub>2</sub>–isoGln); 17.8 (CH<sub>3</sub>–Ala). ESI-MS: m/z 534.0 [M + H]<sup>+</sup>.

4.4.1.3. (4R)-Benzyl 4-{(2S)-[(1'-tert-butyloxycarbonylamino)-ferrocenoylamido] propanoylamido}-4-carbamoylbutanoate (10c). An orange-yellow oil (72.3 mg, 60%).  $R_{\rm f}=0.62$  (CHCl $_{\rm J}/$ 

MeOH, 10:1). IR (CHCl<sub>3</sub>)  $\overline{v}_{max}/cm^{-1}$ : 3436, 3401 w (NH<sub>free</sub>), 3325 m (NH $_{assoc.}$ ), 1737 s, 1679 s, 1635 s (C=O $_{COOEt}$  C=O $_{CONH}$ ), 1520 m (amide II). <sup>1</sup>H NMR (CDCl<sub>3</sub>, 328 K)  $\delta$ /ppm: 7.80 (d, 1H, J = 7.2Hz, NH-isoGln); 6.65 (s, 1H, NH-Ala); 6.11 (s, 1H, NH $_{\rm Boc}$ ); 7.29– 7.25 (m, 6H, Ph, NH<sub>2</sub>-isoGln), 7.18 (s, 1H, Ph); 5.04 (m, 2H, 2  $\times$ CH-Fn); 4.64 (s, 1H, CH-Fn); 4.51 (s, 1H, CH $\alpha$ -isoGln); 4.46–4.41 (m, 1H, CH $\alpha$ -Ala); 4.31 (d, 3H, J = 7.1 Hz, 2 × CH-Fn); 4.25 (d, 2H, I = 8.2 Hz,  $CH_2$ -Ph); 3.90 (s, 1H, CH-Fn); 3.81 (s, 1H, CH-Fn); 2.06-2.41 (m, 2H, CH<sub>2</sub>-isoGln); 2.24-2.21 (m, 1H, CHisoGln); 2.01–1.92 (m, 1H, CH-isoGln); 1.43 (s, 9H,  $3 \times \text{CH}_3$ – Boc); 1.38 (d, 3H, J = 7.1 Hz, CH<sub>3</sub>-Ala). <sup>13</sup>C NMR (DMSO- $d_6$ , 328 K)  $\delta/\text{ppm}$ : 173.0, 172.13, 169.53, 153.05 (C=O); 136.1 (C-Ph); 128.4, 128.0, 127.9 (CH-Ph); 98.0 (C-Fn); 71.9, 71.4, 69.7, 69.6 (CH-Fn); 66.9 (PhCH<sub>2</sub>O); 65.8, 65.3, 62.6, 62.1 (CH-Fn); 53.0  $(CH\alpha-Ala)$ ; 50.5  $(CH\alpha-iGln)$ ; 31.0  $(CH_2-iGln)$ ; 28.6  $(CH_3-Boc)$ ; 26.4 (CH<sub>2</sub>-iGln); 17.2 (CH<sub>3</sub>-Ala). ESI-MS: m/z 635.6 [M + H]<sup>+</sup>. HRMS: m/z [M + Na]<sup>+</sup> Calcd for C<sub>31</sub>H<sub>38</sub>FeN<sub>4</sub>O<sub>7</sub> 657.1990, found 657.1996.

4.4.1.4. (4R)-Benzyl 4-{(2S)-[(1'-amino)ferrocenoylamido]propanoylamido}-4-carbamoyl-butanoate (10g). To a solution of 10c (0.14 mmol) in dry DCM (3 mL) TFA was added (0.2 mL, 2.6 mmol). The reaction mixture was stirred at room temperature for 2.5 h. It was monitored by TLC (CHCl<sub>3</sub>/MeOH, 10:1). After reaction completion, the mixture was evaporated in vacuo and the crude product purified by column chromatography with gradient elution (CHCl<sub>3</sub>/MeOH, 10:1 to 3:1). Aqueous solution of HCOONH<sub>4</sub> (c =0.1 mol dm<sup>-3</sup>) was added to a pure compound and the solution was evaporated in vacuo. Compound 10g was obtained as brown-orange oil (69.6 mg, 93%).  $R_f = 0.29$  (CHCl<sub>3</sub>/MeOH, 10:1). <sup>1</sup>H NMR (CD<sub>3</sub>OD)  $\delta$ /ppm: 7.38–7.29 (m, 5H, Ph); 5.11 (s, 2H, 2 × CH-Fn); 4.80 (s, 1H, CH-Fn); 4.75 (s, 1H, CH-Fn); 4.42–4.33 (m, 4H, CH<sub>2</sub>– Ph, CH $\alpha$ -Ala, CH $\alpha$ -isoGln); 4.04 (s, 1H, CH-Fn); 3.97 (s, 1H, CH-Fn); 3.89 (s, 2H, CH-Fn); 2.52-2.49 (t, 2H, J = 7.2 Hz,  $CH_2$ isoGln); 2.33-2.24 (m, 1H, CH-isoGln); 1.98-1.94 (m, 1H, CHisoGln); 1.42 (d, 3H, J = 7.3 Hz, CH<sub>3</sub>-Ala). <sup>13</sup>C NMR (CD<sub>3</sub>OD)  $\delta$ / ppm: 176.3, 176.2, 174.1, 173.7 (C=O); 137.6 (C-Ph); 129.6, 129.3, 125.2 (CH-Ph); 108.4 (C-Fn); 72.6, 72.3, 70.7, 70.1 (CH-Fn); 67.4 (PhCH<sub>2</sub>O); 66.2, 66.1, 61.2, 60.7 (CH-Fn); 53.7 (CHα-Ala); 51.3 (CHα-isoGln); 31.5 (CH<sub>2</sub>-isoGln); 27.9 (CH<sub>2</sub>-isoGln); 17.6 (CH<sub>3</sub>-Ala). ESI-MS: m/z 535.6 [M + H]<sup>+</sup>. HRMS: m/z [M + H]<sup>+</sup> Calcd for C<sub>26</sub>H<sub>30</sub>FeN<sub>4</sub>O<sub>5</sub> 535.1644, found 535.1642.

4.4.1.5. (2R)-Diethyl-2-{(2S)-[(ferocenoylamido)ethanoylamido]-3-methylbutanoylamido} pentane-1,5-dioate (12a). A yellow solid (65 mg, 60%).  $R_f = 0.22$  (EtOAc/DCM, 5:1). mp = 141.5–144 °C. IR (CHCl<sub>3</sub>)  $\bar{v}_{max}/cm^{-1}$ : 3418 m (NH<sub>free</sub>), 3319 w (NH<sub>assoc</sub>), 1729 s, 1665 s (C=O<sub>COOEt</sub> C=O<sub>CONH</sub>), 1513 m (amide II). <sup>1</sup>H NMR (CDCl<sub>3</sub>)  $\delta$ /ppm: 7.41 (d, 1H, J = 7.5 Hz, NH-Val); 7.32 (d, 1H, J =8.7 Hz, NH-Glu); 7.05 (pt, 1H, J = 5.2 Hz, NH-Gly); 4.76 (s, 2H, 2 × CH-Fn); 4.56–4.54 (m, 1H, CH $\alpha$ -Val); 4.46 (dd, 1H,  $J_1$  = 8.9 Hz,  $J_2$ = 5.9 Hz, CH $\alpha$ -Glu); 4.33 (s, 2H, 2 × CH-Fn); 4.20 (s, 5H, 5 × CH-Fn); 4.19-4.08 (m, 6H,  $2 \times CH_2$ -ethyl,  $CH_2$ -Gly); 2.42-2.37 (m, 2H, CH<sub>2</sub>-Glu); 2.21-2.18 (m, 2H, CH-Glu, CH-Val); 2.02-2.01 (m, 1H, CH-Glu); 1.26–1.21 (m, 6H,  $2 \times \text{CH}_3$ -ethyl); 0.98 (d, 3H, J= 6.9 Hz,  $CH_3-Val$ ); 0.95 (d, 3H, J = 6.9 Hz,  $CH_3-Val$ ). <sup>13</sup>C NMR (CDCl<sub>3</sub>)  $\delta$ /ppm: 172.8, 171.6, 171.4, 171.2, 170.0 (5 × C=O); 75.1 (C-Fn); 70.7, 70.6, 69.8, 68.4 (CH-Fn); 61.5, 60.8 (2  $\times$  CH<sub>2</sub>-ethyl); 58.5 (CH $\alpha$ -Val); 51.9 (CH $\alpha$ -Glu); 43.7 (CH $_{2}$ -Gly); 30.9 (CH-Val); 30.4 (CH<sub>2</sub>-Glu); 26.9 (CH<sub>2</sub>-Glu); 19.4 (CH<sub>3</sub>-Val); 17.9 (CH<sub>3</sub>-Val); 14.2, 14.1 (2 × CH<sub>3</sub>-ethyl). ESI-MS: m/z 572.6 [M + H]<sup>+</sup>. HRMS:  $m/z [M + H]^+$  Calcd for  $C_{27}H_{37}FeN_3O_7$  572.2059, found 572.2059.

4.4.1.6. (2R)-Diethyl-2-{(2S)-[(ferrocenylethanoylamido)-ethanoylamido]-3-methylbutanoyl-amido}pentane-1,5-dioate (12b). A yellow-brown oil (58 mg, 52%).  $R_{\rm f}=0.70$  (CHCl<sub>3</sub>/MeOH, 10:1). IR (CHCl<sub>3</sub>)  $\overline{v}_{\rm max}/{\rm cm}^{-1}$ : 3413 m(NH<sub>free</sub>), 3329 m (NH<sub>assoc.</sub>), 1735 s, 1665 s (C=O<sub>COOEν</sub> C=O<sub>CONH</sub>), 1519 m (amide II). <sup>1</sup>H NMR (CDCl<sub>3</sub>) δ/ppm: 7.19 (d, 1H, J=7.3 Hz, NH-Glu); 6.93 (d, 1H, J=7.4 Hz, NH-Val); 6.64 (d, 1H, J=8.7 Hz, NH-Gly); 4.52–4.50 (m, 1H, CHα-Glu); 4.35 (dd, 1H,  $J_1=8.7$  Hz,  $J_2=5.4$  Hz, CHα-Val); 4.24–4.11 (m, 13H, 9 × CH-Fn, 2 × CH<sub>2</sub>-ethyl); 3.92 (pt, 2H,

CH<sub>2</sub>–Gly); 3.35 (s, 2H, Fn-CH<sub>2</sub>); 2.40–2.34 (m, 2H, CH<sub>2</sub>–Glu); 2.18–2.14 (m, 2H, CH-Glu, CH-Val); 2.0–1.98 (m, 1H, CH-Glu); 1.26–1.22 (m, 6H, 2 × CH<sub>3</sub>-ethyl); 0.96 (d, 3H, J = 6.8 Hz, CH<sub>3</sub>–Val); 0.88 (d, 3H, J = 6.8 Hz, CH<sub>3</sub>–Val). <sup>13</sup>C NMR (CDCl<sub>3</sub>)  $\delta$ /ppm: 173.1, 172.0, 171.6, 170.8, 169.1 (5 × C=O); 80.8 (C-Fn); 69.2, 69.0, 68.6 (CH-Fn); 61.7, 60.9 (2 × CH<sub>2</sub>–ethyl); 58.4 (CH $\alpha$ -Val); 52.0 (CH $\alpha$ -Glu); 43.6 (CH<sub>2</sub>–Gly); 37.6 (Fn-CH<sub>2</sub>); 30.8 (CH-Val); 30.5 (CH<sub>2</sub>–Glu); 27.0 (CH<sub>2</sub>–Glu); 19.3 (CH<sub>3</sub>–Val); 17.4 (CH<sub>3</sub>–Val); 14.3, 14.2 (2 × CH<sub>3</sub>-ethyl). ESI-MS: m/z 586.3 [M + H]<sup>+</sup> HRMS: m/z [M + H]<sup>+</sup> Calcd for C<sub>28</sub>H<sub>39</sub>FeN<sub>3</sub>O<sub>7</sub> 586.2215, found 586.2219.

4.4.1.7. (2R)-diethyl-2-((2S)-{[(1'-tert-butyloxycarbonylamino)ferrocenoylamido]ethanoyl-amido}-3-methylbutanoylamido)pentane-1,5-dioate (12c). An orange-yellow solid (81 mg, 62%).  $R_f =$ 0.28 (EtOAc/DCM, 5:1). mp = 49.5–52 °C. IR (CHCl<sub>3</sub>)  $\overline{v}_{max}/cm^{-1}$ : 3437 sh, 3416 w (NH<sub>free</sub>), 3320 m (NH<sub>assoc.</sub>), 1735 s, 1665 s (C=  $O_{COOE_U}$  C= $O_{CONH}$ ), 1538 m (amide II). H NMR (CDCl<sub>3</sub>)  $\delta$ /ppm, 328 K: 7.06 (d, 1H, J = 6.3 Hz, NH-Boc); 7.05 (d, 1H, J = 6.3 Hz, NH-Val); 6.86 (s, 1H, NH-Glu); 6.79 (s, 1H, NH-Gly); 4.66 (s, 1H, CH-Fn); 4.63 (s, 1H, CH-Fn); 4.59–4.55 (m, 1H, CH $\alpha$ -Val); 4.47 (s, 1H, CH-Fn); 4.45 (s, 1H, CH-Fn); 4.41 (dd, 1H,  $J_1 = 8.9$  Hz,  $J_2 =$ 5.9 Hz, CH $\alpha$ -Glu); 4.36 (s, 2H, 2 × CH-Fn); 4.19–3.99 (m, 8H, 2 ×  $CH_2$ -ethyl,  $CH_2$ -Gly +2 × CH-Fn); 2.42-2.37 (m, 2H,  $CH_2$ -Glu); 2.28-2.19 (m, 2H, CH-Glu, CH-Val); 2.07-2.04 (m, 1H, CH-Glu); 1.59 (s, 9H,  $3 \times \text{CH}_3$ -Boc); 1.27-1.23 (m, 6H,  $2 \times \text{CH}_3$ -ethyl); 0.99 (d, 3H, J = 6.9 Hz,  $CH_3-Val$ ); 0.97 (d, 3H, J = 6.9 Hz,  $CH_3-Val$ ).  $^{13}$ C NMR (CDCl<sub>3</sub>)  $\delta$ /ppm, 328 K: 173.0, 171.8, 171.3, 171.2, 154.0 (C=O); 80.5, 76.6 (C-Fn); 71.4, 71.3, 70.0, 69.5, 65.7, 65.6, 62.4, 62.3 (CH-Fn); 61.8, 60.8 (2 × CH<sub>2</sub>-ethyl); 58.8 (CH $\alpha$ -Val); 52.2 (CHα-Glu); 44.2 (CH<sub>2</sub>-Gly); 30.8 (CH-Val); 30.6 (CH<sub>2</sub>-Glu); 28.6 (CH<sub>3</sub>-Boc)27.2 (CH<sub>2</sub>-Glu); 19.5 (CH<sub>3</sub>-Val); 17.9 (CH<sub>3</sub>-Val); 14.3, 14.2 (2 × CH<sub>3</sub>-ethyl). ESI-MS: m/z 687.5 [M + H]<sup>+</sup>. HRMS: m/z [M + H]<sup>+</sup> Calcd for  $C_{32}H_{46}FeN_4O_9$  687.2692, found 687.2705.

4.4.1.8. (2R)-Diethyl-2-((2S)-{[(1'-benzyloxymethyl)ferrocenoylamido]ethanoylamido}-3-methylbutanoylamido)pentane-1,5-dioate (12d). An orange-yellow oil (92 mg, 70%).  $R_f =$ 0.30 (EtOAc/DCM, 5:1). IR (CHCl<sub>3</sub>)  $\overline{v}_{\rm max}/{\rm cm}^{-1}$ : 3416 m (NH<sub>free</sub>), 3324 m (NH<sub>assoc.</sub>), 1740 s, 1664 s (C= $O_{COOEt}$ , C= $O_{CONH}$ ), 1511 s (amide II).  ${}^{1}$ H NMR (CDCl<sub>3</sub>)  $\delta/ppm$ : 7.36–7.37 (m, 4H, Ph), 7.31– 7.29 (m, 1H, Ph), 7.23 (d, 1H, J = 5.0 Hz, NH-Glu); 7.19 (t, 1H, J =3.6 Hz, NH-Gly); 6.93 (d, 1H, J = 5.8 Hz, NH-Val); 4.68–4.67 (m, 2H, 2 × CH-Fn); 4.58 (s, 2H, CH<sub>2</sub>-Ph), 4.54-4.52 (m, 1H, CH $\alpha$ -Glu); 4.40 (dd, 1H,  $J_1 = 8.7$  Hz,  $J_2 = 3.6$  Hz, CH $\alpha$ -Val); 4.31–4.30 (m, 2H, 2 × CH-Fn); 4.27 (s, 2H, CH<sub>2</sub>Ph); 4.21–4.18 (m, 4H, 4 × CH-Fn); 4.15–4.08 (m, 4H, 2 × CH<sub>2</sub>-ethyl); 3.74 (d, 2H, J = 3.7Hz, CH<sub>2</sub>-Gly); 2.41-2.36 (m, 2H, CH<sub>2</sub>-Glu); 2.26-2.24 (m, 2H, CH-Glu, CH-Val); 2.09-2.02 (m, 1H, CH-Glu); 1.22 (t, 6H, J = 4.8Hz,  $2 \times \text{CH}_3$ -ethyl); 0.96 (d, 3H, J = 4.6 Hz,  $\text{CH}_3$ -Val); 0.92 (d, 3H,  $J = 4.6 \text{ Hz}, \text{ CH}_3 - \text{Val}).$  <sup>13</sup>C NMR (CDCl<sub>3</sub>)  $\delta/\text{ppm}$ : 173.0, 171.8, 171.7, 171.2, 170.0 (5  $\times$  C=O); 138.0 (C-Ph); 128.7, 128.2, 128.1 (CH-Ph); 85.4 (C-Fn); 76.0 (C-Fn); 72.9 (Fn-CH<sub>2</sub>O); 71.0, 70.6, 70.5, 69.9, 69.8, 69.3, 69.2 (CH-Fn); 68.1 (PhCH<sub>2</sub>O); 61.6, 60.8 (2 × CH<sub>2</sub>-ethyl); 58.5 (CH $\alpha$ -Val); 52.0 (CH $\alpha$ -Glu); 43.8 (CH<sub>2</sub>-Gly); 30.7 (CH<sub>2</sub>-Glu); 30.5 (CH-Val); 26.9 (CH<sub>2</sub>-Glu); 19.5 (CH<sub>3</sub>-Val); 17.7 (CH<sub>3</sub>-Val); 14.3, 14.2 (2 × CH<sub>3</sub>-ethyl). ESI-MS: m/z714.6  $[M + Na]^+$ . HRMS:  $m/z [M + Na]^+$  Calcd for  $C_{35}H_{45}FeN_3O_8$ 714.2453, found 714.2446.

4.4.1.9. (2R)-Diethyl-2-((2S)-{[(1'-ethanoylamido)-ferrocenoylamido]ethanoylamido}-3-methylbutanoylamido)-pentane-1,5-dioate (12e). An orange-yellow oil (92 mg, 77%).  $R_f$  = 0.15 (EtOAc/DCM, 5:1). IR (CHCl<sub>3</sub>)  $\bar{v}_{max}/cm^{-1}$ : 3412 w (NH<sub>free</sub>), 3307 m (NH<sub>assoc.</sub>), 1740 s, 1664 s (C=O<sub>COOEt</sub>, C=O<sub>CONH</sub>), 1524 s (amide II). <sup>1</sup>H NMR (CDCl<sub>3</sub>) δ/ppm: 8.59 (s, 1H, NH-Ac); 7.57 (d, 1H, J = 7.52 Hz, NH-Glu); 7.51 (d, 1H, J = 8.8 Hz, NH-Val); 7.24 (pt, 1H, J = 5.6 Hz, NH-Gly); 4.68 (s, 1H, CH-Fn); 4.66 (s, 1H, CH-Fn); 4.63 (s, 1H, CH-Fn); 4.35 (bs, 2H, 2 × CH-Fn); 4.59-4.54 (m, 2H, CH-Fn, CHα-Glu); 4.47 (dd, 1H, J<sub>1</sub> = 8.6 Hz, J<sub>2</sub> = 5.9 Hz, CHα-Val); 4.14-4.07 (m, 6H, 2 × CH-Fn, 2 × CH<sub>2</sub>-ethyl); 3.99 (s, 2H, CH<sub>2</sub>-Gly); 2.41-2.39 (m, 2H, CH<sub>2</sub>-Glu); 2.26-2.17 (m, 2H, CH-

Glu, CH-Val); 2.15–2.03 (m, 4H, CH-Glu, CH<sub>3</sub>–Ac); 1.24–1.21 (m, 6H, 2 × CH<sub>3</sub>-ethyl); 0.98 (d, 3H, J = 6.8 Hz, CH<sub>3</sub>–Val); 0.97 (d, 3H, J = 6.8 Hz, CH<sub>3</sub>–Val); 0.97 (d, 3H, J = 6.8 Hz, CH<sub>3</sub>–Val). <sup>13</sup>C NMR (CDCl<sub>3</sub>)  $\delta$ /ppm: 172.9, 171.8, 171.6, 171.4, 170.7, 169.6 (6 × C=O); 96.1 (C-Fn); 76.2 (C-Fn); 71.4, 71.3, 70.1, 69.4, 65.7, 65.6, 63.4, 63.0 (CH-Fn); 61.8, 60.9 (2 × CH<sub>2</sub>–ethyl); 58.6 (CHα-Val); 52.1 (CHα-Glu); 43.6 (CH<sub>2</sub>–Gly); 31.1 (CH-Val); 30.5 (CH<sub>2</sub>–Glu); 26.9 (CH<sub>2</sub>–Glu); 23.9 (CH<sub>3</sub>–Ac); 19.5 (CH<sub>3</sub>–Val); 18.0 (CH<sub>3</sub>–Val); 14.3, 14.2 (2 × CH<sub>3</sub>-ethyl). ESI-MS: m/z 629.6 [M + H]<sup>+</sup>. HRMS: m/z [M + H]<sup>+</sup> Calcd for C<sub>29</sub>H<sub>40</sub>FeN<sub>4</sub>O<sub>8</sub> 629.2274, found 629.2277.

4.4.1.10. (4R)-tert-butyl 4-{(2S)-[(1'-benzyloxymethyl)ferrocenoylamido]propanoylamido}-4-carbamoylbutanoate (13d). An orange oil (81.7 mg, 71%).  $R_f = 0.48$  (CHCl<sub>3</sub>/MeOH, 10:1). IR (CHCl<sub>3</sub>)  $\overline{v}_{max}/cm^{-1}$ : 3405 m (NH<sub>free</sub>), 3330 m (NH<sub>assoc.</sub>), 1679 s, 1635 s (C=O<sub>COOEt</sub> C=O<sub>CONH</sub>), 1573 m (amide II). <sup>1</sup>H NMR (CDCl<sub>3</sub>, 328 K)  $\delta$ /ppm: 7.47 (d, 1H, J = 8.1 Hz, NH-isoGln); 7.36-7.34 (m, 4H, Ph), 7.31-7.28 (m, 1H, Ph); 6.97 (s, 1H, NH<sub>2</sub>isoGln), 6.83 (d, J = 7.4 Hz, NH-Ala); 5.75 (s, 1H, NH<sub>2</sub>-isoGln), 4.67-4.64 (m, 2H, 2 × CH-Fn); 4.57 (s, 2H, 2 × CH-Fn); 4.47-4.41 (m, H, CH $\alpha$ -isoGln); 4.40–4.37 (m, H, CH $\alpha$ -Ala); 4.31–4.29 (m, 4H,  $2 \times CH_2$ -Ph); 4.26 (s, 2H,  $CH_2$ -Ph); 4.24 (s, 1H, CH-Fn); 4.21-4.19 (s, 3H, 3 × CH-Fn); 2.48-2.32 (m, 2H, CH<sub>2</sub>-isoGln); 2.19-1.96 (m, 1H, CH-isoGln); 2.01-1.96 (m, 1H, CH-isoGln); 1.43 (s, 9H, 3 × CH<sub>3</sub>-tBu); 1.40 (d, 3H, J = 6.8 Hz, CH<sub>3</sub>-Ala). <sup>13</sup>C NMR (CDCl<sub>3</sub>, 328 K)  $\delta$ /ppm: 173.8, 173.4, 173.2, 171.6 (C=O); 138.61 (C-Ph); 128.6, 128.0, 127.9 (CH-Ph); 85.4, 81.4 (C-Fn); 75.1 (C<sub>q</sub>-tBu); 72.5 (Fn-CH<sub>2</sub>O); 71.3, 70.9, 70.7, 70.0, 69.2, 69.1 (CH-Fn); 67.7 (PhCH<sub>2</sub>O); 52.9 (CHα-Ala); 49.9 (CHα-isoGln); 31.2 (CH<sub>2</sub>-iGln); 28.2 (CH<sub>3</sub>-tBu); 27.0 (CH<sub>2</sub>-iGln); 17.9 (CH<sub>3</sub>-Ala). ESI-MS: m/z 643.0 [M+K]<sup>+</sup>. HRMS: m/z [M]<sup>+</sup> Calcd for C<sub>31</sub>H<sub>39</sub>FeN<sub>3</sub>O<sub>6</sub> 605.2188, found 605.2181.

4.5. General Procedure for the Preparation of 11a–c, 12f and 13f. To a solution of 10a-c, 12d or 13d, respectively, (0.087 mmol) in MeOH (15 mL) was added 10% palladium on activated charcoal (0.28 mmol) under hydrogen atmosphere (3 bar). The reaction mixture was stirred for 2 h at room temperature. The reaction was monitored by TLC (EtOAc/DCM, 5:1 for 12d, CHCl<sub>3</sub>/MeOH, 10:1 for all other compounds). After completion of the reaction, the catalyst was filtered off and the remaining solution was evaporated *in vacuo*. The crude products were purified by column chromatography. All compounds, with the exception of 11b, were purified using gradient elution (CHCl<sub>3</sub>/MeOH, 10:1 to 3:1). The peptide 11b was purified using CH<sub>3</sub>CN/MeOH/H<sub>2</sub>O, 5:1:0.7.

4.5.1. (4R)-Carbamoyl-4-[(2S)-(ferrocenoylamido)-propanoylamido]butanoic acid (11a). An orange-yellow oil (33.6 mg, 90%).  $R_f$  = 0.14 (CHCl<sub>3</sub>/MeOH, 10:1). <sup>1</sup>H NMR (CD<sub>3</sub>OD) δ/ppm: 4.48–4.39 (m, 4H, 4 × CH-Fn); 4.26 (s, 5H, 5 × CH-Fn); 2.43 (t, 2H, J = 7.1, CH<sub>2</sub>–isoGln); 2.27–2.25 (m, 1H, CH-isoGln); 1.97–1.95 (m, 1H, CH-isoGln); 1.47 (d, 3H, J = 7.8 Hz, CH<sub>3</sub>–Ala). <sup>13</sup>C NMR (CD<sub>3</sub>OD) δ/ppm: 176.9, 176.5, 175.8, 173.9 (4 × C=O); 75.7 (C-Fn); 72.0, 71.9, 70.9, 69.9, 69.3 (CH-Fn); 53.9 (CHα-Ala); 51.2 (CHα-isoGln); 31.8 (CH<sub>2</sub>–isoGln); 28.2 (CH<sub>2</sub>–isoGln); 17.6 (CH<sub>3</sub>–Ala). ESI-MS: m/z 430.4 [M + H]<sup>+</sup>. HRMS: m/z [M + H]<sup>+</sup> Calcd for C<sub>19</sub>H<sub>23</sub>FeN<sub>3</sub>O<sub>5</sub> 430.1065, found 430.1062.

4.5.2. (4R)-Carbamoyl-4-[(2S)-(ferrocenylethanoylamido)-propanoylamido]butanoic acid (11b). A yellow oil (19.3 mg, 50%).  $R_f = 0.44$  (CH<sub>3</sub>CN/MeOH/H<sub>2</sub>O, 5:1:0.7). <sup>1</sup>H NMR (DMSO- $d_6$ ) δ/ppm: 12.08 (s, 1H, COOH); 8.10 (m, 2H, NH-Ala, NH-isoGln); 7.30 (s, 1H, NH<sub>2</sub>-isoGln); 7.11 (s, 1H, NH<sub>2</sub>-isoGln); 4.25–4.05 (m, 11H, CHα-Ala, CHα-isoGln, 9 × CH-Fn); 3.18–3.16 (m, 2H, CH<sub>2</sub>-Fn); 2.20 (t, 2H, J = 7.8 Hz, CH<sub>2</sub>-isoGln); 2.02–1.94 (m, 1H, CH-isoGln); 1.74–1.65 (m, 1H, CH-isoGln); 1.22 (d, 3H, J = 7.0 Hz, CH<sub>3</sub>-Ala). <sup>13</sup>C NMR (DMSO- $d_6$ ) δ/ppm: 175.4, 174.0, 172.8, 170.4 (4 × C=O); 83.1 (C-Fn); 69.0, 68.9, 67.6 (CH-Fn); 52.9 (CHα-isoGln); 49.1 (CHα-Ala); 36.6 (CH<sub>2</sub>-Fn); 32.6, 28.0 (CH<sub>2</sub>-isoGln); 18.5 (CH<sub>3</sub>-Ala). ESI-MS: m/z 466.0 [M + Na]<sup>+</sup>. HRMS: m/z [M + H]<sup>+</sup> Calcd for C<sub>20</sub>H<sub>25</sub>FeN<sub>3</sub>O<sub>5</sub> 443.1144, found 443.1144.

4.5.3. (4R)-{(2S)-[(1'-tert-butyloxycarbonylamino)-ferrocenoylamido]propanoylamido}-4-carbamoylbutanoic acid

(11c). An orange oil (43.6 mg, 92%).  $R_{\rm f}=0.11$  (CHCl<sub>3</sub>/MeOH, 10:1). <sup>1</sup>H NMR (CD<sub>3</sub>OD)  $\delta$ /ppm: 4.79 (m, 2H, 2 × CH-Fn); 4.51–4.38 (m, 6H, CH $\alpha$ -isoGln, CH $\alpha$ -Ala, 4 × CH-Fn); 4.07–4.04 (m, 2H, 2 × CH-Fn); 2.40–2.35 (m, 2H, CH<sub>2</sub>-isoGln); 2.29–2.24 (m, 1H, CH-isoGln); 1.97–1.96 (m, 1H, CH-isoGln); 1.53–1.50 (m, 12H, 3 × CH<sub>3</sub>–Boc, CH<sub>3</sub>–Ala). <sup>13</sup>C NMR (CD<sub>3</sub>OD)  $\delta$ /ppm: 175.7, 174.6 (C=O); 154.3 (C=O, Boc); 97.9 (C-Fn); 79.5 (C-Boc); 75.0 (C-Fn); 71.7, 71.5, 69.2, 65.6, 65.5, 61.7 (CH-Fn); 53.2 (CH $\alpha$ -Ala); 50.0 (CH $\alpha$ -isoGln); 32.6 (CH<sub>2</sub>-isoGln); 27.5 (CH<sub>2</sub>-isoGln); 27.3 (CH<sub>3</sub>–Boc); 16.2 (CH<sub>3</sub>–Ala). ESI-MS: m/z 567.5 [M + Na]<sup>+</sup>. HRMS: m/z [M]<sup>+</sup> Calcd for C<sub>24</sub>H<sub>32</sub>FeN<sub>4</sub>O<sub>7</sub> 544.1620, found 544.1618.

4.5.4. (2R)-Diethyl-2-((2S)-{[(1'-hydroxymethyl)ferrocenoylamido]ethanoylamido}-3-methylbutanoylamido)pentane-1,5-dioate (12f). An orange-yellow oil (39.2 mg, 75%).  $R_f$  = 0,15 (EtOAc/DCM, 5:1). IR (CHCl<sub>3</sub>)  $\overline{v}_{\rm max}/{\rm cm}^{-1}$ : 3414 m (NH<sub>free</sub>), 3314 m (NH<sub>assoc.</sub>), 1734 s, 1664 s (C= $O_{COOEv}$  C= $O_{CONH}$ ), 1511 s (amide II).  $^{1}$ H NMR (CDCl<sub>3</sub>)  $\delta$ /ppm: 7.35 (t, 1H, J = 5.3 Hz, NH-Gly); 7.27 (d, 1H, J = 7.5 Hz, NH-Glu); 7.12 (d, 1H, J = 8.7 Hz, NH-Val); 4.70 (s, 2H, 2 × CH-Fn); 4.59–4.53 (m, 1H, CH $\alpha$ -Glu); 4.43 (dd, 1H,  $J_1 = 8.6$  Hz,  $J_2 = 5.6$  Hz, CH $\alpha$ -Val); 4.35 (bs, 2H, 2 × CH-Fn); 4.24-4.10 (m, 10H,  $4 \times \text{CH-Fn}$ ,  $2 \times \text{CH}_2$ -ethyl,  $\text{CH}_2$ -OH); 2.41-2.37 (m, 2H, CH<sub>2</sub>-Glu); 2.25-2.18 (m, 2H, CH-Glu, CH-Val); 2.04-2.00 (m, 1H, CH-Glu); 1.25-1.21 (m, 6H, 2 × CH<sub>3</sub>ethyl); 0.98 (d, 3H, J = 6.9 Hz,  $CH_3-Val$ ); 0.95 (d, 3H, J = 6.9 Hz, CH<sub>3</sub>–Val).  $^{13}$ C NMR (CDCl<sub>3</sub>)  $\delta$ /ppm: 173.0, 171.7, 171.6, 171.3, 170.0 (5 × C=O); 85.2 (C-Fn); 76.1 (C-Fn); 71.0, 70.6, 70.6, 70.2, 69.9, 69.2, 69.1 (CH-Fn); 61.6, 60.8 (2 × CH<sub>2</sub>-ethyl); 58.6 (Fn-CH<sub>2</sub>); 58.4 (CHα-Val); 52.0 (CHα-Glu); 44.0 (CH<sub>2</sub>-Gly); 30.8 (CH-Val); 30.5 (CH<sub>2</sub>-Glu); 27.0 (CH<sub>2</sub>-Glu); 19.5 (CH<sub>3</sub>-Val); 17.9 (CH<sub>3</sub>-Val); 14.3, 14.2 (2 × CH<sub>3</sub>-ethyl). ESI-MS: m/z 584.6  $[M-OH]^+$ . HRMS: m/z  $[M-OH]^+$  Calcd for  $C_{28}H_{39}FeN_3O_8$ 584.2054, found 584.2072.

4.5.5. (4R)-tert-Butyl 4-carbamoyl-4-{(2S)-[(1'-hydroxymethyl)-ferrocenoylamido] propanoylamido}butanoate (13f). A brownyellow oil (40.3 mg, 75%).  $R_{\rm f}=0.39$  (CHCl<sub>3</sub>/MeOH, 10:1).  $^{\rm l}$ H NMR (CD<sub>3</sub>OD)  $\delta$ /ppm: 4.82–4.80 (m, 1H, CH<sub>2</sub>–OH); 4.45–4.35 (m, 4H, 2 × CH-Fn, CHα-isoGln, CHα-Ala), 4.30–4.24 (m, 4H, 4 × CH-Fn), 4.20 (s, 2H, 2 × CH-Fn); 2.37–2.33 (m, 2H, CH<sub>2</sub>-isoGln); 2.21–2.21 (m, 1H, CH-isoGln); 1.90–1.86 (m, 1H, CH-isoGln); 1.40 (m, 12H, CH<sub>3</sub>-fBu, CH<sub>3</sub>–Ala).  $^{\rm l3}$ C NMR (CD<sub>3</sub>OD)  $\delta$ /ppm: 176.5, 175.8, 173.9, 173.5 (C=O); 85.6, 81.8 (C-Fn); 76.6 (C(CH<sub>3</sub>)<sub>3</sub>-Boc); 72.5, 72.4, 72.3, 72.2, 71.4 (CH-Fn); 71.2 (CH<sub>2</sub>OH); 70.4, 69.9 (CH-Fn); 53.6 (CHα-Ala); 51.2 (CHα-isoGln); 32.7 (CH<sub>2</sub>-isoGln); 28.4 (C(CH<sub>3</sub>)<sub>3</sub>-Boc); 28.1 (CH<sub>2</sub>-isoGln); 17.8 (CH<sub>3</sub>-Ala). ESI-MS: m/z 498.2 [M-OH]<sup>+</sup>. HRMS: m/z [M-OH]<sup>+</sup> Calcd for C<sub>24</sub>H<sub>33</sub>FeN<sub>3</sub>O<sub>6</sub> 498.1719, found 498.1710.

**4.6. Biological Evaluation.** *4.6.1. HEK-Blue NOD2 Cells.* HEK-Blue hNOD2 cells (Invivogen, San Diego, CA) were maintained in Dulbecco's modified Eagle's medium (Sigma-Aldrich, St. Louis, MO), adhering to the manufacturer's instructions. The culture medium was supplemented with 10% heat-inactivated fetal bovine serum (Gibco), 2 mM L-glutamine (Sigma-Aldrich), 100 U/mL penicillin (Sigma-Aldrich), 100  $\mu$ g/mL streptomycin (Sigma-Aldrich), and 100  $\mu$ g/mL normocin (Invivogen) for the initial two passages. For subsequent passages, the medium was further supplemented with 30  $\mu$ g/mL blasticidin (Invivogen) and 100  $\mu$ g/mL zeocin (Invivogen). Cell cultures were maintained in a humidified atmosphere at 37 °C with 5% CO<sub>2</sub>.

4.6.2. Peripheral Blood Mononuclear Cells. PBMCs were isolated from heparinized blood of healthy, consenting donors using density gradient centrifugation with Ficoll-Paque (Pharmacia, Sweden). Postisolation, the cells were resuspended in RPMI 1640 medium (Sigma-Aldrich, St. Louis, MO) supplemented with 10% heatinactivated fetal bovine serum (Gibco), 2 mM L-glutamine (Sigma-Aldrich), 100 U/mL penicillin (Sigma-Aldrich), and 100  $\mu$ g/mL streptomycin (Sigma-Aldrich) for further assays.

4.6.3. Metabolic Activity. The substances being studied were first dissolved in DMSO and then diluted in the culture medium to achieve the required final concentrations, making sure that the DMSO

concentration remained below 0.1%. HEK-Blue hNOD2 cells were seeded at a density of 40,000 cells per well in 96-well plates, each well containing 100  $\mu\rm L$  of culture medium. The cells were then exposed to 20  $\mu\rm M$  of each compound or to the corresponding vehicle (0.1% DMSO; control cells). After an 18-h incubation period at 37 °C with 5% CO $_2$  metabolic activity was assessed using the CellTiter 96 Aqueous One Solution cell proliferation assay (Promega, Madison, WI), according to the manufacturer's instructions. Each experiment was performed in duplicate and repeated three times as independent biological replicates.

4.6.4. Measurement of NF-κB Transcriptional Activity (HEK-Blue Detection). The HEK-Blue hNOD2 cell line reporter assay was developed by cotransfecting HEK293 cells with the hNOD2 gene and an NF-κB-inducible secreted embryonic alkaline phosphatase (SEAP) reporter gene. Activation of NOD2 leads to NF-kB-mediated production of SEAP, which can be quantitatively measured using a colorimetric assay. For the assay, HEK-Blue hNOD2 cells were plated at a density of 25,000 cells per well in 96-well plates with 100  $\mu L$  of HEK-Blue detection medium (Invivogen, San Diego, CA). The cells were then treated with various concentrations of the compounds (7– 8 different concentrations ranging from 1 nM to 20  $\mu$ M) or the vehicle control (0.1% DMSO) to determine EC<sub>50</sub> values. Following an 18-h incubation at 37 °C with 5% CO<sub>2</sub>, SEAP activity was measured spectrophotometrically at an absorbance of 630 nm (BioTek Synergy microplate reader; Winooski, VT). EC<sub>50</sub> values were calculated using Prism software (version 10; GraphPad Software, CA). Each experiment was performed in duplicate and repeated in at least three independent biological replicates.

4.6.5. Cytokine Release from Peripheral Blood Mononuclear *Cells.* PBMCs were seeded at a density of  $1 \times 10^6$  cells/mL in 96-well plates, each well containing 100  $\mu \rm L$  of growth medium. The cells were treated with MDP and compound 12b (1  $\mu$ M) or the corresponding vehicle control (0.1% DMSO), both in the absence and presence of LPS (20 ng/mL). After an 18-h incubation period at 37  $^{\circ}$ C with 5% CO<sub>2</sub>, cell-free supernatants were harvested and stored at -80 °C until analysis. Cytokine production was measured using the LEGENDplex Human Essential Immune Response Panel (Biolegend) on an Attune NxT flow cytometer (Thermo Fisher Scientific, Waltham, MA). Standard curves were generated using recombinant cytokines included in the kit. Data analysis was performed using Biolegend software Qognit and Prism (GraphPad, San Diego, CA) software. Experiments were performed in duplicate and repeated as two independent biological replicates. Statistical significance was assessed using oneway ANOVA followed by Dunnett's multiple comparisons test.

4.6.6. Statistics. The data were analyzed using Prism software (version 10; GraphPad Software, CA). Statistical significance was determined according to the specific procedures outlined in each experiment.

#### ASSOCIATED CONTENT

#### Supporting Information

The Supporting Information is available free of charge at https://pubs.acs.org/doi/10.1021/acs.organomet.5c00312.

<sup>1</sup>H NMR spectra, <sup>13</sup>C NMR spectra; <sup>1</sup>H–<sup>1</sup>H NOESY spectra, <sup>1</sup>H–<sup>1</sup>H COSY spectra, <sup>1</sup>H–<sup>1</sup>H HMQC spectra, <sup>1</sup>H–<sup>13</sup>C HMBC spectra; concentration- and temperature-dependent IR spectra; temperature- and solvent-dependent <sup>1</sup>H NMR spectra, concentration-dependent NH chemical shifts; HRMS and HPLC-ESI data; EC<sub>50</sub> curves of most potent desmuramylpeptides **12a**–**f** and reference compounds **MDP** and **SG8** (PDF)

#### AUTHOR INFORMATION

#### **Corresponding Authors**

Ziga Jakopin — Department of Pharmaceutical Chemistry, Faculty of Pharmacy, University of Ljubljana, 1000 Ljubljana, Slovenia; o orcid.org/0000-0001-9384-0858; Email: Ziga.Jakopin@ffa.uni-lj.si

Lidija Barišić — Department of Chemistry and Biochemistry, University of Zagreb Faculty of Food Technology and Biotechnology, 10000 Zagreb, Croatia; orcid.org/0000-0002-4310-4198; Email: lidija.barisic@pbf.unizg.hr

#### **Authors**

**Željka** Car – Department of Chemistry, University of Zagreb Faculty of Science, 10000 Zagreb, Croatia

Monika Kovačević – Department of Chemistry and Biochemistry, University of Zagreb Faculty of Food Technology and Biotechnology, 10000 Zagreb, Croatia

Vesna Petrović Peroković – Department of Chemistry, University of Zagreb Faculty of Science, 10000 Zagreb, Croatia

Karla Čižmešija – Division of Organic Chemistry and Biochemistry, Ruđer Bošković Institute, 10000 Zagreb, Croatia

Rosana Ribić – University North, University Center Varaždin, 42000 Varaždin, Croatia; orcid.org/0000-0001-7611-538X

Špela Janež – Department of Pharmaceutical Chemistry, Faculty of Pharmacy, University of Ljubljana, 1000 Ljubljana, Slovenia

Complete contact information is available at: https://pubs.acs.org/10.1021/acs.organomet.5c00312

#### **Author Contributions**

The manuscript was written through contributions of all authors. All authors have given approval to the final version of the manuscript.

#### Notes

The authors declare no competing financial interest.

#### ACKNOWLEDGMENTS

This work was supported by the Croatian Science Foundation under the project number IP-2020-02-9162 and Slovenian Research and Innovation Agency (P1-0420, J3-4496).

#### REFERENCES

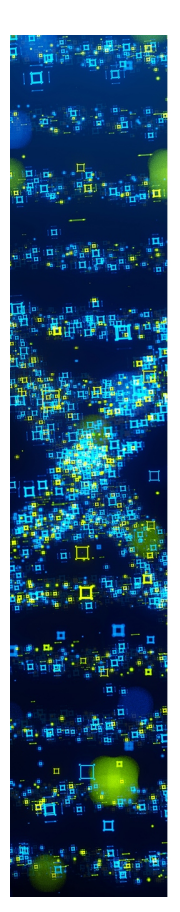
- (1) Astruc, D. Why Is Ferrocene so Exceptional? *Eur. J. Inorg. Chem.* **2017**, 2017 (1), 6–29.
- (2) Wu, G.-l.; Tan, S.; Tan, X.; Chen, G.; Yang, Q. Recent Advances in Ferrocene-Based Nanomedicines for Enhanced Chemodynamic Therapy. *Theranostics* **2025**, *15* (2), 384–407.
- (3) Edwards, E. I.; Epton, R.; Marr, G. 1,1'-Ferrocenyldiacetic acid anhydride and its use in the preparation of heteroannularly substituted ferrocenyl-penicillins and -cephalosporins. *J. Organomet. Chem.* 1976, 122, C49–C53.
- (4) Patra, M.; Gasser, G. The medicinal chemistry of ferrocene and its derivatives. *Nat. Rev. Chem.* **2017**, *1*, No. 0066.
- (5) Top, S.; Dauer, B.; Vaissermann, J.; Jaouen, G. Facile Route to Ferrocifen, 1-[4-(2-Dimethylaminoethoxy)]-1-(Phenyl-2-Ferrocenylbut-1-Ene), First Organometallic Analogue of Tamoxifen, by the McMurry Reaction. *J. Organomet. Chem.* **1997**, *541* (1), 355–361.
- (6) Biot, C.; Glorian, G.; Maciejewski, L. A.; Brocard, J. S.; et al. Synthesis and Antimalarial Activity in Vitro and in Vivo of a New Ferrocene-Chloroquine Analogue. *J. Med. Chem.* **1997**, *40* (23), 3715–3718.
- (7) Sharma, B.; Kumar, V. Has Ferrocene Really Delivered Its Role in Accentuating the Bioactivity of Organic Scaffolds? *J. Med. Chem.* **2021**, *64* (23), 16865–16921.

- (8) Ludwig, B. S.; Correia, J. D. G.; Kühn, F. E. Ferrocene Derivatives as Anti-Infective Agents. *Coord. Chem. Rev.* **2019**, 396, 22–48.
- (9) Miguel, S.; Ortín-Fernández, J.; Gómez-Pastor, S.; Moliné, M. Á.; Sánchez-Murcia, P. A.; Corral, I.; Sanz-Rodríguez, F.; González-Vadillo, A. M. Reimagining Pt(II) Anticancer Agents: The Role of Ferrocene in Monofunctional Chemotherapeutic Compounds. *Inorg. Chem.* 2025, 64 (23), 11497–11509.
- (10) Sharma, A.; Rana, R.; Kumar, N.; gulati, H. k.; Jyoti; Khanna, A.; Sharma, S.; Pooja; Singh, J. V.; Bedi, P. M. S. Ferrocene-Based Compounds: Promising Anticancer and Antimalarial Agents in Modern Therapeutics. *Med. Chem. Res.* **2025**, 34 (6), 1177–1199.
- (11) Gupta, P.; Madhavan, S.; Kapur, M. Synthesis of Ferrocene 1,3-Derivatives by Distal C-H Activation. *Angew. Chem., Int. Ed.* **2023**, 62 (34), No. e202305278.
- (12) Čakić Semenčić, M.; Kovačević, M.; Barišić, L. Recent Advances in the Field of Amino Acid-Conjugated Aminoferrocenes—A Personal Perspective. *Int. J. Mol. Sci.* **2024**, 25 (9), No. 4810.
- (13) Čakić Semenčić, M.; Barišić, L. Ferrocene Bioconjugates. *Croat. Chem. Acta* **2017**, 90 (4), 537–569.
- (14) Kovačević, M.; Kodrin, I.; Cetina, M.; Kmetič, I.; Murati, T.; Semenčić, M. Č.; Roca, S.; Barišić, L. The Conjugates of Ferrocene-1,1'-Diamine and Amino Acids. A Novel Synthetic Approach and Conformational Analysis. *Dalton Trans.* **2015**, *44* (37), 16405–16420.
- (15) Kovačević, M.; Molčanov, K.; Radošević, K.; Srček, V. G.; Roca, S.; Čače, A.; Barišić, L. Conjugates of 1'-Aminoferrocene-1-Carboxylic Acid and Proline: Synthesis, Conformational Analysis and Biological Evaluation. *Molecules* **2014**, *19* (8), 12852–12880.
- (16) Kovač, V.; Radošević, K.; Bebek, A.; Makarević, J.; Štefanić, Z.; Barišić, L.; Žinić, M.; Rapić, V. The First Oxalamide-Bridged Ferrocene: Facile Synthesis, Preliminary Conformational Analysis and Biological Evaluation. *Appl. Organomet. Chem.* **2017**, *31* (7), No. e3653.
- (17) Kovačević, M.; Markulin, D.; Zelenika, M.; Marjanović, M.; Lovrić, M.; Polančec, D.; Ivančić, M.; Mrvčić, J.; Molčanov, K.; Milašinović, V.; Roca, S.; Kodrin, I.; Barišić, L. Hydrogen Bonding Drives Helical Chirality via 10-Membered Rings in Dipeptide Conjugates of Ferrocene-1,1'-Diamine. *Int. J. Mol. Sci.* 2022, 23 (20), No. 12233.
- (18) Kovačević, M.; Čakić Semenčić, M.; Radošević, K.; Molčanov, K.; Roca, S.; Šimunović, L.; Kodrin, I.; Barišić, L. Conformational Preferences and Antiproliferative Activity of Peptidomimetics Containing Methyl 1'-Aminoferrocene-1-Carboxylate and Turn-Forming Homo- and Heterochiral Pro-Ala Motifs. *Int. J. Mol. Sci.* 2021, 22 (24), No. 13532.
- (19) Kovač, V.; Kodrin, I.; Radošević, K.; Molčanov, K.; Adhikari, B.; Kraatz, H.-B.; Barišić, L. Oxalamide-Bridged Ferrocenes: Conformational and Gelation Properties and In Vitro Antitumor Activity. *Organometallics* **2022**, *41* (8), 920–936.
- (20) Raičević, V.; Jovanović, L.; Rodić, M. V.; Stojanović, N.; Ćulum, A. S.; Radulović, N. Homopregnane-Type Ferrocene-Steroid Conjugates Exhibit Immunomodulatory Activity. *Bioorg. Chem.* **2025**, *155*, No. 108129.
- (21) Liu, X.; Wang, H.; Li, Z.; Li, J.; He, S.; Hu, C.; Song, Y.; Gao, H.; Qin, Y. Transformable Self-Delivered Supramolecular Nanomaterials Combined with Anti-PD-1 Antibodies Alleviate Tumor Immunosuppression to Treat Breast Cancer with Bone Metastasis. *J. Nanobiotechnol.* **2024**, 22 (1), No. 566.
- (22) Silva, L. P.; Santos, I. P.; Silva, D. K. C.; Dos Reis, B. P. Z. C.; Meira, C. S.; Castro, M. V. B. d. S.; Dos Santos Filho, J. M.; Araujo-Neto, J. H. d.; Ellena, J. A.; Silveira, R. G. d.; Soares, M. B. P. Molecular Hybridization Strategy on the Design, Synthesis, and Structural Characterization of Ferrocene-N-Acyl Hydrazones as Immunomodulatory Agents. *Molecules* **2022**, 27 (23), No. 8343.
- (23) Maekawa, S.; Ohto, U.; Shibata, T.; Miyake, K.; Shimizu, T. Crystal Structure of NOD2 and Its Implications in Human Disease. *Nat. Commun.* **2016**, *7*, No. 11813.

- (24) Guryanova, S. V. Regulation of Immune Homeostasis via Muramyl Peptides-Low Molecular Weight Bioregulators of Bacterial Origin. *Microorganisms* **2022**, *10* (8), No. 1526.
- (25) Dubé, J.-Y.; Behr, M. A. A Nod to the Bond between NOD2 and Mycobacteria. *PLoS Pathog.* **2023**, *19* (6), No. e1011389.
- (26) Maršavelski, A.; Paurević, M.; Ribić, R. Mannosylated Adamantane-Containing Desmuramyl Peptide Recognition by the NOD2 Receptor: A Molecular Dynamics Study. *Org. Biomol. Chem.* **2021**, *19* (32), 7001–7012.
- (27) Lauro, M. L.; D'Ambrosio, E. A.; Bahnson, B. J.; Grimes, C. L. Molecular Recognition of Muramyl Dipeptide Occurs in the Leucine-Rich Repeat Domain of Nod2. *ACS Infect. Dis.* **2017**, 3 (4), 264–270.
- (28) Griffin, M. E.; Hespen, C. W.; Wang, Y.-C.; Hang, H. C. Translation of Peptidoglycan Metabolites into Immunotherapeutics. *Clin. Transl. Immunol.* **2019**, *8* (12), No. e1095.
- (29) Jakopin, Ż.; Corsini, E.; Gobec, M.; Mlinarič-Raščan, I.; Dolenc, M. S. Design, Synthesis and Biological Evaluation of Novel Desmuramyldipeptide Analogs. *Eur. J. Med. Chem.* **2011**, 46 (9), 3762–3777.
- (30) Ribić, R.; Paurević, M.; Tomić, S. Advances in Desmuramyl Peptide Research. *Croat. Chem. Acta* **2019**, 92 (2), 153–161.
- (31) Khan, F.-A.; Ulanova, M.; Bai, B.; Yalamati, D.; Jiang, Z.-H. Design, Synthesis and Immunological Evaluation of Novel Amphiphilic Desmuramyl Peptides. *Eur. J. Med. Chem.* **2017**, *141*, 26–36.
- (32) Guzelj, S.; Bizjak, Š.; Jakopin, Ž. Discovery of Desmuramylpeptide NOD2 Agonists with Single-Digit Nanomolar Potency. ACS Med. Chem. Lett. 2022, 13 (8), 1270–1277.
- (33) Guzelj, S.; Nabergoj, S.; Gobec, M.; Pajk, S.; Klančič, V.; Slütter, B.; Frkanec, R.; Štimac, A.; Šket, P.; Plavec, J.; Mlinarič-Raščan, I.; Jakopin, Ž. Structural Fine-Tuning of Desmuramylpeptide NOD2 Agonists Defines Their In Vivo Adjuvant Activity. *J. Med. Chem.* **2021**, *64* (11), 7809–7838.
- (34) Janež, Š.; Guzelj, S.; Kocbek, P.; de Vlieger, E. A.; Slütter, B.; Jakopin, Ž. Distinctive Immune Signatures Driven by Structural Alterations in Desmuramylpeptide NOD2 Agonists. *J. Med. Chem.* **2024**, *67* (19), 17585–17607.
- (35) Peroković, V. P.; Kovačević, M.; Paurević, M.; Bušljeta, M.; Car, Ž.; Ribić, R.; Barišić, L. Ferrocene Derivatives of Desmuramyl Peptide: Synthesis, Conformational Properties, and Interactions with NOD2 Receptor. *Polyhedron* **2025**, *274*, No. 117516.
- (36) Singh, A.; Lumb, I.; Mehra, V.; Kumar, V. Ferrocene-appended pharmacophores: an exciting approach for modulating the biological potential of organic scaffolds. *Dalton Trans.* **2019**, *48*, 2840–2860.
- (37) Ribić, R.; Habjanec, L.; Vranešić, B.; Frkanec, R.; Tomić, S. Synthesis and Immunostimulating Properties of Novel Adamant-1-Yl Tripeptides. *Chem. Biodiversity* **2012**, 9 (4), 777–788.
- (38) Ribić, R.; Stojković, R.; Milković, L.; Antica, M.; Cigler, M.; Tomić, S. Design, Synthesis and Biological Evaluation of Immunostimulating Mannosylated Desmuramyl Peptides. *Beilstein Arch.* **2019**, 2019 (1), No. 8.
- (39) Haris, P. I.; Chapman, D. The Conformational Analysis of Peptides Using Fourier Transform IR Spectroscopy. *Biopolymers* 1995, 37 (4), 251–263.
- (40) Vass, E.; Hollósi, M.; Besson, F.; Buchet, R. Vibrational Spectroscopic Detection of Beta- and Gamma-Turns in Synthetic and Natural Peptides and Proteins. *Chem. Rev.* **2003**, *103* (5), 1917–1954.
- (41) Ramos, S.; Thielges, M. C. Site-Specific 1D and 2D IR Spectroscopy to Characterize the Conformations and Dynamics of Protein Molecular Recognition. *J. Phys. Chem. B* **2019**, 123 (17), 3551–3566.
- (42) Jagesar, D. C.; Hartl, F.; Buma, W. J.; Brouwer, A. M. Infrared Study of Intercomponent Interactions in a Switchable Hydrogen-Bonded Rotaxane. *Chem. Eur. J.* **2008**, *14* (6), 1935–1946.
- (43) Joseph, J.; Jemmis, E. D. Red-, Blue-, or No-Shift in Hydrogen Bonds: A Unified Explanation. *J. Am. Chem. Soc.* **2007**, *129* (15), 4620–4632.
- (44) Arunan, E.; Desiraju, G. R.; Klein, R. A.; Sadlej, J.; Scheiner, S.; Alkorta, I.; Clary, D. C.; Crabtree, R. H.; Dannenberg, J. J.; Hobza, P.; Kjaergaard, H. G.; Legon, A. C.; Mennucci, B.; Nesbitt, D. J.

- Definition of the hydrogen bond (IUPAC Recommendations 2011). *Pure Appl. Chem.* **2011**, 83 (8), 1637–1641.
- (45) Fornaro, T.; Burini, D.; Biczysko, M.; Barone, V. Hydrogen-Bonding Effects on Infrared Spectra from Anharmonic Computations: Uracil—Water Complexes and Uracil Dimers. *J. Phys. Chem. A* **2015**, 119 (18), 4224–4236.
- (46) Barth, A. Infrared Spectroscopy of Proteins. *Biochim. Biophys. Acta, Bioenerg.* **2007**, *1767* (9), 1073–1101.
- (47) Kaplan, S.; Colak, M.; Hosgoren, H.; Pirinccioglu, N. Design of L-Lysine-Based Organogelators and Their Applications in Drug Release Processes. *ACS Omega* **2019**, *4* (7), 12342–12356.
- (48) Berger, N.; Wollny, L. J. B.; Sokkar, P.; Mittal, S.; Mieres-Perez, J.; Stoll, R.; Sander, W.; Sanchez-Garcia, E. Solvent-Enhanced Conformational Flexibility of Cyclic Tetrapeptides. *ChemPhysChem* **2019**, 20 (13), 1664–1670.
- (49) Nerli, S.; McShan, A. C.; Sgourakis, N. G. Chemical Shift-Based Methods in NMR Structure Determination. *Prog. Nucl. Magn. Reson. Spectrosc.* **2018**, *106*–*107*, 1–25.
- (50) Pardi, A.; Wagner, G.; Wüthrich, K. Protein Conformation and Proton Nuclear-Magnetic-Resonance Chemical Shifts. *Eur. J. Biochem.* 1983, 137 (3), 445–454.
- (51) Gellman, S. H.; Dado, G. P.; Liang, G. B.; Adams, B. R. Conformation-Directing Effects of a Single Intramolecular Amide-Amide Hydrogen Bond: Variable-Temperature NMR and IR Studies on a Homologous Diamide Series. *J. Am. Chem. Soc.* **1991**, *113* (4), 1164–1173.
- (52) Kovačević, M.; Čakić Semenčić, M.; Kodrin, I.; Roca, S.; Perica, J.; Mrvčić, J.; Stanzer, D.; Molčanov, K.; Milašinović, V.; Brkljačić, L.; Barišić, L. Biological Evaluation and Conformational Preferences of Ferrocene Dipeptides with Hydrophobic Amino Acids. *Inorganics* **2023**, *11* (1), No. 29.
- (53) Raghothama, S. R.; Awasthi, S. K.; Balaram, P.  $\beta$ -Hairpin Nucleation by Pro-Gly  $\beta$ -Turns. Comparison of D-Pro-Gly and L-Pro-Gly Sequences in an Apolar Octapeptide. *J. Chem. Soc., Perkin Trans.* 2 **1998**, *1*, 137–144.
- (54) Chen, B.; Nie, H.; Hu, R.; Qin, A.; Zhao, Z.; Tang, B. Z. Insights into the Correlation between the Molecular Conformational Change and AIE Activity of 2,5-Bis(Dimesitylboryl)-3,4-Diphenylsiloles. *J. Mater. Chem. C* **2016**, 4 (32), 7541–7545.
- (55) Vincenzi, M.; Mercurio, F. A.; Leone, M. NMR Spectroscopy in the Conformational Analysis of Peptides: An Overview. *Curr. Med. Chem.* **2021**, 28 (14), 2729–2782.
- (56) Liu, J.-Y.; Sun, X.-Y.; Tang, Q.; Song, J.-J.; Li, X.-Q.; Gong, B.; Liu, R.; Lu, Z.-L. An Unnatural Tripeptide Structure Containing Intramolecular Double H-Bonds Mimics a Turn Hairpin Conformation. *Org. Biomol. Chem.* **2021**, *19* (19), 4359–4363.
- (57) Stevens, E. S.; Sugawara, N.; Bonora, G. M.; Toniolo, C. Conformational Analysis of Linear Peptides. 3. Temperature Dependence of NH Chemical Shifts in Chloroform. *J. Am. Chem. Soc.* **1980**, 102 (23), 7048–7050.
- (58) Andersen, N. H.; Neidigh, J. W.; Harris, S. M.; Lee, G. M.; Liu, Z.; Tong, H. Extracting Information from the Temperature Gradients of Polypeptide NH Chemical Shifts. 1. The Importance of Conformational Averaging. *J. Am. Chem. Soc.* 1997, 119 (36), 8547–8561.
- (59) Baxter, N. J.; Williamson, M. P. Temperature Dependence of 1H Chemical Shifts in Proteins. *J. Biomol. NMR* **1997**, *9* (4), 359–369.
- (60) Cierpicki, T.; Zhukov, I.; Byrd, R. A.; Otlewski, J. Hydrogen Bonds in Human Ubiquitin Reflected in Temperature Coefficients of Amide Protons. *J. Magn. Reson.* **2002**, *157* (2), 178–180.
- (61) Kovačević, M.; Kodrin, I.; Roca, S.; Molčanov, K.; Shen, Y.; Adhikari, B.; Kraatz, H.-B.; Barišić, L. Helically Chiral Peptides That Contain Ferrocene-1,1'-Diamine Scaffolds as a Turn Inducer. *Chem. Eur. J.* **2017**, 23 (43), 10372–10395.
- (62) Chatterjee, B.; Saha, I.; Raghothama, S.; Aravinda, S.; Rai, R.; Shamala, N.; Balaram, P. Designed Peptides with Homochiral and Heterochiral Diproline Templates as Conformational Constraints. *Chem. Eur. J.* **2008**, *14* (20), 6192–6204.

- (63) Kovačević, M.; Čakić Semenčić, M.; Bagović, M.; Radošević, K.; Hanousek Čiča, K.; Mrvčić, J.; Molčanov, K.; Roca, S.; Kodrin, I.; Barišić, L. Hydrogen Bond Patterning and Biological Activity of Ferrocene Conjugates with Homo- and Heterochiral Ala–Pro Dipeptides. *Organometallics* **2024**, *43* (20), 2608–2625.
- (64) van Der Meer, J. H. M.; Netea, M. G.; Dinarello, C. A. Modulation of Muramyl Dipeptide Stimulation of Cytokine Production by Blood Components. *Clin. Exp. Immunol.* **2009**, *156* (3), 428–433.
- (65) Traub, S.; von Aulock, S.; Hartung, T.; Hermann, C. Invited Review: MDP and Other Muropeptides Direct and Synergistic Effects on the Immune System. *J. Endotoxin Res.* **2006**, *12* (2), 69–85.
- (66) Netea, M. G.; Ferwerda, G.; de Jong, D. J.; Jansen, T.; Jacobs, L.; Kramer, M.; Naber, T. H. J.; Drenth, J. P. H.; Girardin, S. E.; Jan Kullberg, B.; Adema, G. J.; Van der Meer, J. W. M. Nucleotide-Binding Oligomerization Domain-2 Modulates Specific TLR Pathways for the Induction of Cytokine Release 1. *J. Immunol.* 2005, 174 (10), 6518–6523.
- (67) Gobec, M.; Tomašič, T.; Štimac, A.; Frkanec, R.; Trontelj, J.; Anderluh, M.; Mlinarič-Raščan, I.; Jakopin, Ž. Discovery of Nanomolar Desmuramylpeptide Agonists of the Innate Immune Receptor Nucleotide-Binding Oligomerization Domain-Containing Protein 2 (NOD2) Possessing Immunostimulatory Properties. *J. Med. Chem.* **2018**, *61* (7), 2707–2724.
- (68) Lednicer, D.; Lindsay, J. K.; Hauser, C. R. Reaction of the Methiodide of N,N-Dimethylaminomethylferrocene with Potassium Cyanide to Form Ferrocylacetonitrile<sup>1</sup>. *J. Org. Chem.* **1958**, 23 (5), 653–655.
- (69) Barišić, L.; Rapić, V.; Kovač, V. Ferrocene Compounds. XXIX.\* Efficient Syntheses of 1'-Aminoferrocene-1-Carboxylic Acid Derivatives. *Croat. Chem. Acta* **2002**, 75 (1), 199–210. https://hrcak.srce.hr/127496.



CAS BIOFINDER DISCOVERY PLATFORM™

# STOP DIGGING THROUGH DATA —START MAKING DISCOVERIES

CAS BioFinder helps you find the right biological insights in seconds

Start your search

